Iron and Cobalt Ethylene Polymerization Catalysts Bearing 2,6-Bis(Imino)Pyridyl Ligands: Synthesis, Structures, and Polymerization Studies

George J. P. Britovsek,[†] Michael Bruce,[†] Vernon C. Gibson,*[,†] Brian S. Kimberley,[‡] Peter J. Maddox,[‡] Sergio Mastroianni,[†] Stuart J. McTavish,[†] Carl Redshaw,[†] Gregory A. Solan,[†] Staffan Strömberg,[†] Andrew J. P. White,[†] and David J. Williams[†]

Department of Chemistry, Imperial College, South Kensington, London SW7 2AY, U.K., BP Amoco Chemicals Ltd., Sunbury Research Centre, Chertsey Road, Sunbury on Thames, Middlesex TW16 7LN, UK.

Received February 12, 1999

Abstract: The synthesis, characterization, and ethylene polymerization behavior of a series of iron and cobalt halide complexes, LMX_n (M = Fe, X = Cl, n = 2, 3, X = Br, n = 2; M = Co, X = Cl, n = 2), bearing chelating 2,6-bis(imino)pyridyl ligands L [L = 2,6-$(ArNCR^1)_2C_5H_3N$] is reported. X-ray diffraction studies show the geometry at the metal centers to be either distorted square pyramidal or distorted trigonal bipyramidal. Treatment of the complexes LMX_n with methylaluminoxane (MAO) leads to highly active ethylene polymerization catalysts converting ethylene to highly linear polyethylene (PE). $LFeX_2$ precatalysts with ketimine ligands (R^1 = Me) are approximately an order of magnitude more active than precatalysts with aldimine ligands (R^1 = H). Catalyst productivities in the range 3750−20600 g/mmol·h·bar are observed for Fe-based ketimine catalysts, while Co ketimine systems display activities of 450−1740 g/mmol·h·bar. Molecular weights (M_w) of the polymers produced are in the range 14000−611000. Changing reaction conditions also affects productivity and molecular weight; in some systems, a bimodal molecular weight distribution is observed. On the basis of evidence gathered to date, the lower molecular weight fraction is a result of chain transfer to aluminum while the higher molecular weight fraction is produced by a combination of mainly β-H transfer and some chain transfer to aluminum.

1. Introduction

Dramatic advances in metallocene catalyst technology beginning in the early 1980s have impacted the polyolefins industry and resulted in a number of new commercial processes for the preparation of polyolefinic materials with new or improved performance parameters.[1−7] In order to extend the range of polyolefinic materials produced, considerable effort has been devoted to the discovery of new families of catalysts. Of particular interest are those catalysts that allow either for greater control over the resultant polymer properties of established polyolefinic materials or for the production of new materials.[8,9]

An important advance in late transition metal polymerization catalyst technology was described by Brookhart and co-workers, who showed that Ni(II) and Pd(II) complexes incorporating bulky α-diimine ligands are capable of polymerizing ethylene and α-olefins to high molar mass polymers.[10−14] These catalyst systems also incorporate polar monomers such as methyl acrylate into ethylene and propylene copolymers, albeit with relatively low productivities.[11,15,16]

The idea that late transition metal chelate complexes could polymerize α-olefins has stimulated a search for other late-transition metal polymerization catalysts; key advances have recently been reviewed.[17] We were attracted by the potential for using iron as a polymerization active center due to its low cost and ready availability. In parallel studies, Brookhart, DuPont, and this group have reported highly active ethylene polymerization catalysts based on iron(II) and cobalt(II) bearing 2,6-bis(imino)pyridyl ligands.[18−23]

* To whom correspondence should be addressed. E-mail: V.Gibson@ic.ac.uk.

[†] Imperial College.

[‡] BP Amoco Chemicals Ltd.

(1) Brintzinger, H. H.; Fischer, D.; Mülhaupt, R.; Rieger, B.; Waymouth, R. M. *Angew. Chem., Int. Ed. Engl.* **1995**, *34*, 1143−1170.

(2) Bochmann, M. *J. Chem. Soc., Dalton Trans.* **1996**, 255−270.

(3) Jordan, R. F. *Adv. Organomet. Chem.* **1991**, *32*, 325−387.

(4) Fink, G.; Mülhaupt, R.; Brintzinger, H. H. *Ziegler Catalysts: Recent Scientific Innovations and Technological Improvement*; Springer-Verlag: Berlin, Germany, 1995.

(5) Thayer, A. M. *Chem. Eng. News* **1995**, *Sept 11*, 15−20.

(6) Sinclair, K. B.; Wilson, R. B. *Chem. Ind.* **1994**, 857−862.

(7) Havan, R. G. *Chem. Ind.* **1997**, 212.

(8) Kaminsky, W. *Macromol. Chem. Phys.* **1996**, *197*, 3907−3945.

(9) Suhm, J.; Heinemann, J.; Wörner, C.; Müller, P.; Stricker, F.; Kressler, J.; Okuda, J.; Mülhaupt, R. *Macromol. Symp.* **1998**, *129*, 1−28.

(10) Johnson, L. K.; Killian, C. M.; Brookhart, M. *J. Am. Chem. Soc.* **1995**, *117*, 6414−6415.

(11) Johnson, L. K.; Mecking, S.; Brookhart, M. *J. Am. Chem. Soc.* **1996**, *118*, 267−268.

(12) Killian, C. M.; Tempel, D. J.; Johnson, L. K.; Brookhart, M. *J. Am. Chem. Soc.* **1996**, *118*, 11664.

(13) Johnson, L. K.; Killian, C. M.; Arthur, S. D.; Feldman, J.; McCord, E. F.; McLain, S. J.; Kreutzer, K. A.; Bennett, M. A.; Coughlin, E. B.; Ittel, S. D.; Parthasarathy, A.; Tempel, D. J.; Brookhart, M. S. (DuPont), WO 96/23010, **1996** [*Chem. Abstr.* **1996**, *125*, 222773t].

(14) Schleis, T.; Spaniol, T. P.; Okuda, J.; Heinemann, J.; Mülhaupt, R. *J. Organomet. Chem.* **1998**, *569*, 159−167.

(15) Mecking, S.; Johnson, L. K.; Wang, L.; Brookhart, M. *J. Am. Chem. Soc.* **1998**, *120*, 888.

(16) Heinemann, J.; Mülhaupt, R.; Brinkmann, P.; Luinstra, G. *Macromol. Chem. Phys.* **1999**, *200*, 384−389.

(17) Britovsek, G. J. P.; Gibson, V. C.; Wass, D. F. *Angew. Chem., Int. Ed. Engl.* **1999**, *38*, 428−447.

(18) Small, B. L.; Brookhart, M. *Polym. Prepr. (Am. Chem. Soc., Div. Polym. Chem.)* **1998**, *39*, 213.

(19) Small, B. L.; Brookhart, M.; Bennett, A. M. A. *J. Am. Chem. Soc.* **1998**, *120*, 4049−4050.

10.1021/ja990449w CCC: $18.00
Published on Web 09/11/1999

Scheme 1[a]

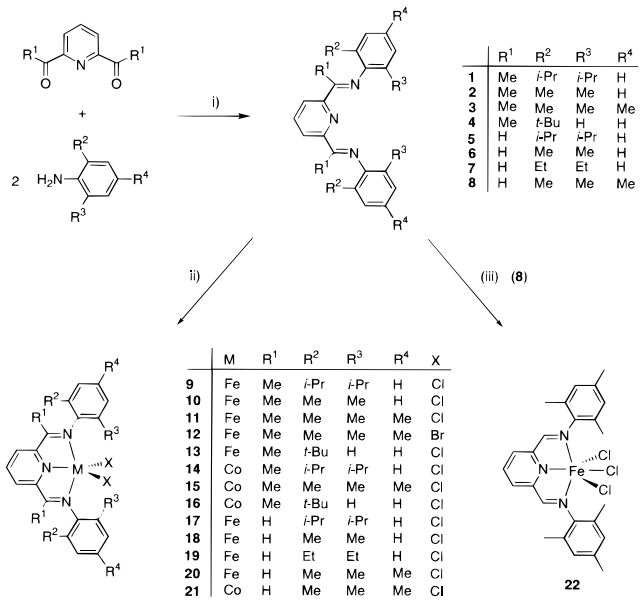

	R^1	R^2	R^3	R^4
1	Me	*i*-Pr	*i*-Pr	H
2	Me	Me	Me	H
3	Me	Me	Me	Me
4	Me	*t*-Bu	H	H
5	H	*i*-Pr	*i*-Pr	H
6	H	Me	Me	H
7	H	Et	Et	H
8	H	Me	Me	Me

	M	R^1	R^2	R^3	R^4	X
9	Fe	Me	*i*-Pr	*i*-Pr	H	Cl
10	Fe	Me	Me	Me	H	Cl
11	Fe	Me	Me	Me	Me	Cl
12	Fe	Me	Me	Me	Me	Br
13	Fe	Me	*t*-Bu	H	H	Cl
14	Co	Me	*i*-Pr	*i*-Pr	H	Cl
15	Co	Me	Me	Me	Me	Cl
16	Co	Me	*t*-Bu	H	H	Cl
17	Fe	H	*i*-Pr	*i*-Pr	H	Cl
18	Fe	H	Me	Me	H	Cl
19	Fe	H	Et	Et	H	Cl
20	Fe	H	Me	Me	Me	Cl
21	Co	H	Me	Me	Me	Cl

[a] Reagents and Conditions: (i) EtOH, H^+; (ii) MCl_2, *n*-BuOH, Δ; (iii) $FeCl_3$, MeCN

In this report we describe the full characterization of iron(II)-, iron(III)-, and cobalt(II)-based precatalysts and the resultant polyolefinic materials produced. Modification in metal center and ligand architecture results in changes in polymerization activity and polymer molecular weight. We also report the effects observed on variation of the reaction conditions, such as the concentration of methylaluminoxane (MAO), the time of reaction, the pressure of ethylene, and the temperature of polymerization.

2. Results

2.1. Synthesis and Characterization. The 2,6-bis(imino)pyridyl ligands **1**-**8**, 2,6-$(ArNCR^1)_2C_5H_3N$, were prepared in high yield from the condensation of two equivalents of the appropriate aniline with one equivalent of either 2,6-diacetylpyridine or 2,6-pyridinedicarboxaldehyde (Scheme 1). The 2,6-bis(imino)pyridyl ligands **1**−**8** may be classified by the nature of R^1 into ketimine (R^1 = Me, **1**−**4**) and aldimine (R^1 = H, **5**−**8**) ligands. Compounds **1**−**8** were characterized by microanalysis, ^{1}H, ^{13}C NMR, and mass spectrometry (see Experimental Section).

The complexes **9**−**21** were synthesized in good yield by treating MX_2 (M = Fe, Co; X = Cl, Br) with the corresponding 2,6-bis(imino)pyridyl ligand in *n*-butanol at elevated temperature, while the Fe(III) complex **22** was prepared by treatment of $FeCl_3$ with **8** in acetonitrile (Scheme 1).

All the complexes, **9**−**22**, were characterized by a variety of techniques including microanalysis, FAB mass spectrometry, UV−vis spectroscopy, magnetic susceptibility, and ^{1}H NMR spectroscopy. In addition, complexes **9**, **11**, **12**, and **14** were subject to single-crystal X-ray diffraction studies.

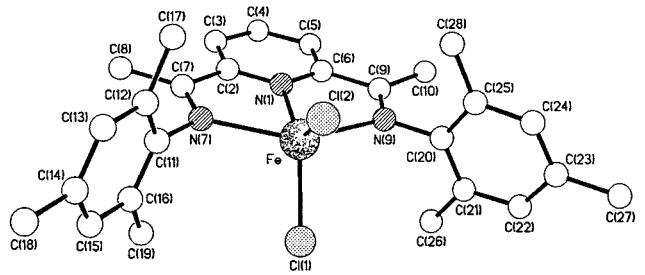

Figure 1. Molecular structure of **11** (isomorphous with the bromide analogue **12**).

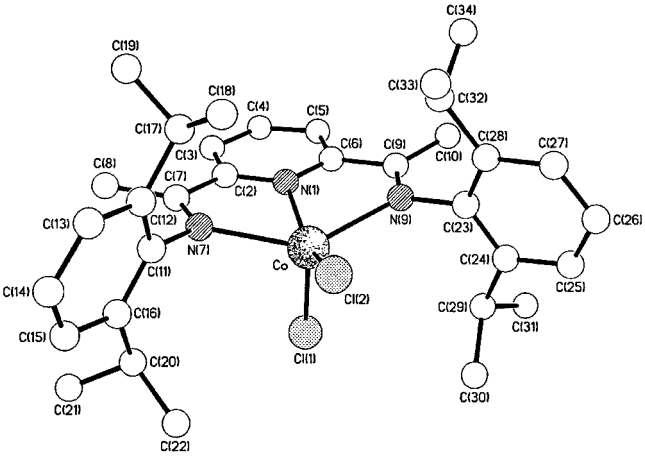

Figure 2. Molecular structure of the cobalt complex **14** (isomorphous with the iron analogue **9**).

Table 1. Selected Bond Lengths (Å) and Angles (Degrees) for Complexes **9**, **11**, **12**, and **14**

	9 [M = Fe, X = Cl]	**11** [M = Fe, X = Cl]	**12** [M = Fe, X = Br]	**14** [M = Co, X = Cl]
M−N(1)	2.088(4)	2.110(6)	2.103(6)	2.051(3)
M−N(7)	2.238(4)	2.271(6)	2.271(6)	2.211(3)
M−N(9)	2.250(4)	2.266(5)	2.260(6)	2.211(3)
M−X(1)	2.311(2)	2.312(2)	2.452(2)	2.293(1)
M−X(2)	2.266(2)	2.278(2)	2.418(2)	2.251(1)
C(7)−N(7)	1.285(6)	1.276(9)	1.269(11)	1.277(5)
C(9)−N(9)	1.280(6)	1.280(8)	1.283(10)	1.280(5)
N(1)−M−N(7)	73.2(1)	72.7(2)	72.8(2)	74.0(1)
N(1)−M−N(9)	72.9(1)	73.0(2)	72.9(2)	74.0(1)
N(7)−M−N(9)	140.1(1)	145.5(2)	145.4(3)	141.3(1)
N(1)−M−X(1)	94.6(1)	118.9(2)	118.7(2)	92.9(1)
N(7)−M−X(1)	100.6(1)	102.4(2)	102.5(2)	100.6(1)
N(9)−M−X(1)	102.5(1)	96.7(1)	97.0(2)	102.3(1)
N(1)−M−X(2)	147.9(1)	131.3(2)	132.3(2)	150.6(1)
N(7)−M−X(2)	98.6(1)	97.8(2)	98.3(2)	98.29(8)
N(9)−M−X(2)	98.9(1)	102.3(2)	102.0(2)	98.84(8)
X(1)−M−X(2)	117.5(1)	109.9(1)	109.1(1)	116.5(1)

Crystals of **9**, **11**, **12**, and **14** suitable for X-ray structural determination were grown from a layered CH_2Cl_2-pentane (1:1) solution (**9**), from acetonitrile (**11**, **12**), or from a concentrated CH_2Cl_2 solution (**14**). The molecular structures of the iron complex **11** (isomorphous with **12**) and the cobalt complex **14** (isomorphous with **9** which has been communicated previously[22]) are shown in Figures 1 and 2, respectively, and selected bond lengths and angles are presented in Table 1.

All four structures are closely related and possess approximate, non-crystallographic C_s symmetry about a plane bisecting the central pyridine ring and containing the metal atom and the two halogen atoms. In each complex the M−N(pyridyl) bond is significantly shorter than the M−N(imino) bonds, with the formal double bond character of the imino linkages N(7)−

(20) Bennett, A. M. A. (DuPont), WO 98/27124, **1998** [*Chem. Abstr.* **1998**, *129*, 122973x].
(21) Bennett, A. M. A. *CHEMTECH* **1999**, *July*, 24−28.
(22) Britovsek, G. J. P.; Gibson, V. C.; Kimberley, B. S.; Maddox, P. J.; McTavish, S. J.; Solan, G. A.; White, A. J. P.; Williams, D. J. *Chem. Commun.* **1998**, 849−850.
(23) Britovsek, G. J. P.; Dorer, B. A.; Gibson, V. C.; Kimberley, B. S.; Solan, G. A. (BP Chemicals Ltd.), WO 99/12981, **1999** [*Chem. Abstr.* **1999**, *130*, 252793].

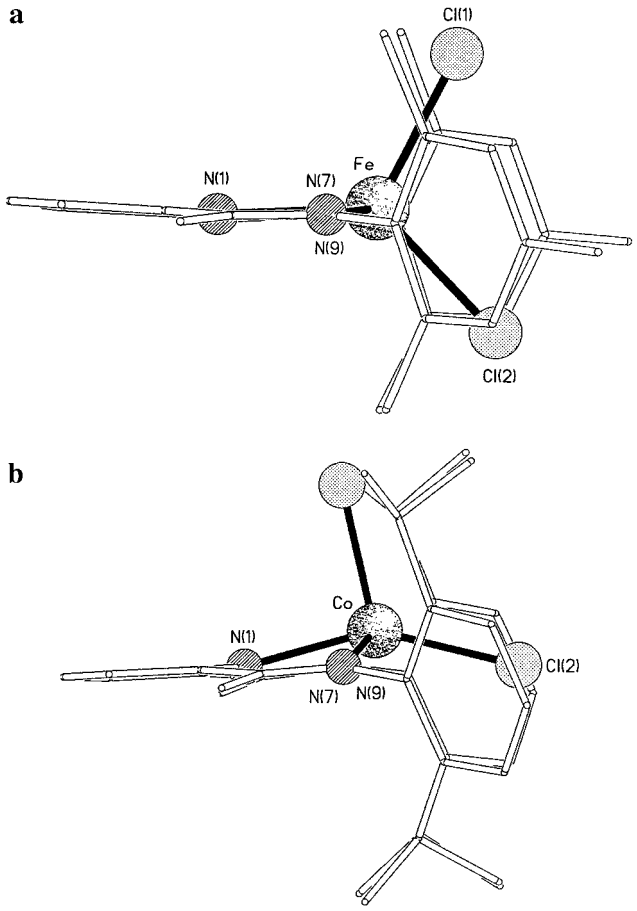

Figure 3. Side-on views, perpendicular to the plane of the three ligand nitrogen atoms, of (**a**) the $FeCl_2$ complex **11** and (**b**) the $CoCl_2$ complex **14**, showing the pronounced differences in coordination geometry and the deviation of the metal centers from the ligand plane.

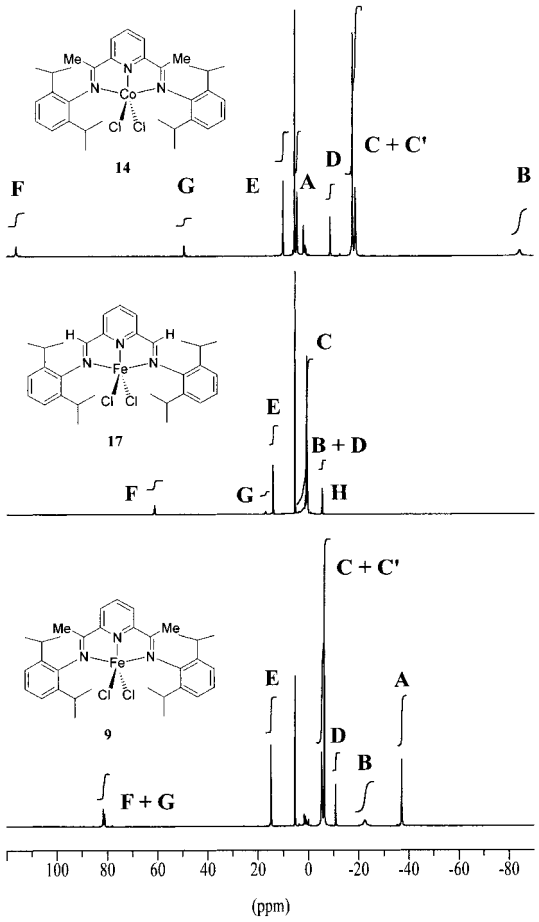

Figure 4. ^{1}H NMR spectra of isostructural **9** and **14** along with the corresponding iron aldimine complex **17** in CD_2Cl_2 at 293 K.

C(7) and N(9)−C(9) having been retained [C═N distances in the range 1.269(11)−1.285(6) Å]. Regardless of whether the substituents on the bis(imino)pyridine ligand backbone are 2,6-diisopropylphenyl [**9** and **14**] or 2,4,6-trimethylphenyl [**11** and **12**], the planes of the phenyl rings are oriented essentially orthogonal to the plane of the backbone [ranging between 77° and 90°], the latter being coplanar to within 0.03−0.07 Å. The principal differences between the 2,6-diisopropylphenyl- and 2,4,6-trimethylphenyl-containing complexes are in the deviation of the metal atom from the N_3 ligand plane and the distortions from square pyramidal geometry at the metal center; indeed the 2,4,6-trimethylphenyl derivatives can be better regarded as trigonal bipyramidal. The deviation of the metal from the N_3 ligand plane is noticeably greater in the 2,6-diisopropylphenyl species than in the 2,4,6-trimethylphenyl complexes with the metal displaced by 0.56 Å for both **9** and **14** but by only 0.09 and 0.10 Å for **11** and **12**, respectively. The differences in geometry between the two pairs of compounds can best be appreciated in Figure 3, parts a and b, which provide views down the N(7)···N(9) vector for one of each isomorphous pair (**11** and **14**, respectively). The different geometries, square pyramidal for **14** and trigonal bipyramidal for **11**, can clearly be seen, as can the very different angles subtended at the metal centers by the pyridyl nitrogen N(1) and the two halogen substituents; similarly the X−M−X angles differ markedly (Table 1). Inspection of space-filling models does not reveal any dominant steric interactions that can be considered to contribute to the two very different geometries observed. Likewise, there are no C−H···X contacts indicative of strong intramolecular hydrogen bonding. Perhaps the only relevant observation is that the "basal" halogen atom X(2) is in each case sandwiched between nonsubstituted phenyl carbon atoms.

The Fe and Co complexes exhibit different electronic environments. All of the complexes are paramagnetic. The Fe(II) complexes afford magnetic moments of ∼5.3 BM, consistent with four unpaired electrons, while the Co(II) complexes have moments of ∼4.6 BM, consistent with three unpaired electrons (Evans NMR method and Evans Balance method[24,25]).

Although the complexes are paramagnetic, ^{1}H NMR spectroscopy can be informative. Figure 4 shows the ^{1}H NMR spectra of the isostructural Fe and Co ketimine complexes **9** and **14** along with the related iron aldimine complex **17**. The spectra of **9** and **14** show 8 paramagnetically shifted peaks that can be assigned, on the basis of integration and proximity to the paramagnetic center, to ketimine protons (**A** = NC*Me*), isopropyl protons (**B** = C*H*Me$_2$, **C** and **C′** = CH*Me*$_2$), aromatic protons (**D** = H_p, **E** = H_m), and pyridyl protons (**F** = H_m, **G** = H_p). Contrastingly, the spectrum of **17** shows 7 broad peaks that can be assigned to isopropyl protons (**B** = C*H*Me$_2$, **C** = CH*Me*$_2$), aromatic protons (**D** = H_p, **E** = H_m), pyridyl protons (**F** = H_m, **G** = H_p), and the aldimine protons (**H** = C*H*═N). A key difference between the ketimine species (**9**, **14**) and the aldimine species (**17**) is the presence of two singlets for the CH*Me*$_2$ protons (**C** and **C′**) in **9** and **14**, while in **17** only one singlet is observed (**C**).

(24) Evans, D. F. *J. Chem. Soc.* **1959**, 2003−2005.
(25) Evans, D. F.; Jakubovic, D. A. *J. Chem. Soc., Dalton Trans.* **1988**, 2927−2933.

Table 2. Results of Ethylene Polymerization Runs with Precatalysts **9**−**22**[a]

run	procatalyst (μmol)	MAO (mmol/ equiv)	yield (g)	activity (g/mmol·h·bar)	M_w[b]	M_n[b]	M_w/M_n[b]	M_{pk}[b] peak 1	M_{pk}[b] peak 2	saturated chain ends[c]	i-propyl chain ends[c]	unsaturated chain ends[c]	unsaturated chain ends[d]
1	**9**[e] (0.5)	0.5/1000	26.9	5340	611000	64000	9.5	246000			polymer insoluble		0.3
2	**10**[e] (0.6)	0.6/1000	56.5	9340	242000	9600	25.3	16000		1.2	0.6	0.6	*f*
3	**11**[e] (0.6)	0.6/1000	123.5[g]	20600	148000	14000	10.7	41000		0.7	0.2	0.5	*f*
4	**12**[e] (0.7)	0.7/1000	122.8[g]	17550	141000	13000	10.8	34000		0.9	0.5	0.7	*f*
5	**13**[e] (0.6)	0.6/1000	22.8	3750	313000	3000	105.1	840	10000	2.0	1.3	0.5	*f*
6	**14**[e] (0.6)	0.6/1000	3.7	450	14000	4200	3.3	12000		2.4	-	1.9	*f*
7	**15**[e] (0.6)	0.6/1000	10.2	1700	257000	1800	144.5	1400	74400	5.9	-	5.2	6.7
8	**16**[e] (0.6)	0.6/1000	10.7	1740	234000	54000	2.3	397000			polymer insoluble		0.2
9	**17**[h] (6)	1.2/200	18.2	305	132000	3400	38.9	3400		2.8	-	2.3	2.8
10	**18**[h] (6)	1.2/200	33.7	560	108000	1900	57.3	1600	105000	5.6	-	5.6	*f*
11	**19**[h] (6)	1.2/200	20.3	340	230000	3900	58.4	4600	85000	2.8	-	2.1	*f*
12	**20**[h] (6)	1.2/200	32.8	550	152000	1800	83.5	1400	110000	5.5	-	5.1	*f*
13	**21**[h] (6)	1.2/200	20.5	340	1600	630	2.6	580		16.3	-	17.1	*f*
14	**22**[h] (6)	1.2/200	26.4	435	112000	1600	70.5	1100	129000	6.4	-	6.2	*f*

[a] Isobutane solvent, 10 bar of ethylene, reaction time 1 h. [b] Determined by GPC at 135 °C. [c] Results from ^{13}C NMR analysis, given per 1000 carbon atoms. [d] Results from IR analysis, given per 1000 carbon atoms. [e] 50 °C, triisobutylaluminum scavenger. [f] Not recorded. [g] 35 °C, trimethylaluminum scavenger. [h] Mass transport problems may have occurred.

The complexes are all intensely colored. In particular, the Fe(II)-ketimines (**9**−**13**) are all blue in color while the Fe(II)-aldimine (**17**−**20**) species are green−brown. A common feature of these iron species is a strong absorption in their UV−vis spectra at ∼700 nm (λ_{max}).

2.2. Polymerization of Ethylene. 2.2.1. General. On treatment with methylaluminoxane (MAO), all of the complexes **9**−**22** are active ethylene polymerization catalysts. Table 2 lists the results of ethylene polymerization runs (1−14) with iron and cobalt precatalysts **9**−**22**. These catalyst systems do not show any induction period; conversely, an immediate exotherm is generally observed. During the polymerization reaction a decrease in activity is noticed, the final activity being typically 10−20% of the initial activity. When these complexes are combined with other Lewis acidic cocatalysts, including diethylaluminum chloride, triethylaluminum, and combinations of triisobutylaluminum/tris(pentafluorophenyl)borane, active polymerization catalysts also result;[26] however, we will focus on MAO-cocatalyzed polymerizations here.

Catalysts were tested under two different sets of polymerization conditions. Cobalt and iron catalysts with ketimine ligands ($R^1 = CH_3$, **9**−**16**) were tested at 10 bar of ethylene at 50 °C for 1 h, employing 1000 equiv of MAO and using triisobutylaluminum as the scavenger (Table 2, runs 1−8). The aldimine-based Fe and Co catalysts ($R^1 = H$, **17**−**22**) displayed relatively low activities under the conditions employed in runs with ketimine catalysts. For this reason, Fe and Co aldimine-derived catalysts were tested at 10 times the catalyst loading, at a slightly lower temperature (35 °C), and with trimethylaluminum as the scavenger (Table 2, runs 9−14), affording overall more optimal conditions for these systems.

To probe the nature of the polymerization reaction, we carried out polymerizations over ranges of activator concentration, reaction time, pressure, and temperature. The following subsections detail the results observed on precatalyst modifications and the effect of varying the polymerization reaction conditions.

2.2.2. Effect of the Metal Center in the Polymerization of Ethylene. The nature of the metal center has a large influence on catalyst productivity. In general, Fe catalysts are more active than the corresponding Co analogues (Table 2, Fe, runs 1−3; Co, runs 6−8); under the conditions reported here, the most active Fe ketimine catalyst is complex **11** (20600 g/mmol·h·bar),[27] while the most active Co ketimine catalyst is complex **16** (1740 g/mmol·h·bar). For the aldimine-derived catalysts, Fe precatalyst **20** displays a productivity of 550 g/mmol·h·bar (Table 2, run 12), while the corresponding Co precatalyst **21** shows a lower productivity of 340 g/mmol·h·bar (Table 2, run 13).

The metal center also influences molecular weight. Fe precatalysts **9**, **11,** and **13** yield M_w's in the range 148000−611000. These Fe compounds share the same corresponding ligand environments as Co precatalysts **14**−**16**, which yield lower M_w's in the range 14000−257000.

Compounds **20** and **22** possess identical ligand environments, but **20** is based on Fe(II) with two ancillary chlorides, while **22** is Fe(III) with three ancillary chlorides. Polymerization tests with these related compounds (Table 2, runs 12, 14) reveal similar productivities of 550 g/mmol·h·bar for **20** and 435 g/mmol·h·bar for **22** and polymer products with similar molecular weights and chain end types (Table 2).

NMR spectroscopy was used to analyze the polyethylene produced by the Fe and Co catalyst systems. NMR analysis of the polymers arising from both Fe- and Co-based precatalysts **9**−**22** reveals highly linear polyethylene.[28] ^{13}C NMR end group analysis of the polymers generated from Fe-based precatalysts reveals saturated end groups in addition to low levels of vinyl unsaturation (Table 2), whereas for all the Co precatalysts, the ratio of vinyl end groups/methyl end groups is approximately 1:1, consistent with one saturated chain end and one unsaturated chain end.

2.2.3. Ligand Backbone Modification. Changes in the ligand environments [2,6-$(ArNCR^1)_2C_5H_3$] of these systems result in changes in catalyst productivity and polymer molecular weight. Changing the substituent on the imine functional group from a ketimine ($R^1 = CH_3$, **9**−**16**) to an aldimine ($R^1 = H$, **17**−**22**) results in differences in productivity, molecular weight, and molecular weight distribution.

Ketimine catalysts are more productive than their aldimine analogues. Fe-based ketimine precatalysts **9**−**11** give productivities in the range 5340−20600 g/mmol·h·bar (Table 2, runs 1−3). The corresponding aldimines **17**, **18**, and **20** display lower productivities in the range 305−560 g/mmol·h·bar (Table 2, runs 9, 10, 12).

(26) Gibson, V. C. Unpublished results.

(27) This catalyst has been optimized to a higher activity since our preliminary report (ref 22).

(28) Roberts, G. C. K. *NMR of Macromolecules: A Practical Approach*; IRC Press: Oxford, U.K., 1993.

NMR analysis of the resultant polymers reveals that Fe-based ketimine precatalysts produce polymers both with isopropyl end groups (triisobutylaluminum is employed as a reactor scavenger) and with a greater number of saturated end groups than vinyl end groups (Table 2). For example, precatalyst **10** (Table 2, run 2) yields PE with small amounts of isopropyl chain ends and a ratio of unsaturated end groups to saturated end groups of 1:2. Fe-based aldimine catalysts produce, at 10 bar ethylene pressure, polymers with a slight excess of saturated to unsaturated end groups, whereas at lower pressure (1 bar) a more substantial excess of saturated chain ends is observed. A 1:1 ratio of saturated to unsaturated end groups is observed for all Co precatalysts, irrespective of the ligand environment.

^{1}H- and ^{13}C NMR analysis yields information on polymers for which M_n is smaller than 30 000.[28] To determine the end groups of higher molecular weight chains, we employed IR spectroscopy.[29] The intensity of the peak at 910 cm^{-1} can be used to give an indication of the number of unsaturated end groups. A series of samples that could be analyzed by NMR spectroscopy was also analyzed by IR spectroscopy (Table 2), revealing good correlation between IR and NMR spectroscopy for low molecular weight samples. A series of samples of $1800 < M_n < 54000$ analyzed by this method indicated the vinyl unsaturation at levels of 0.2−6.7 per 1000 carbon atoms. This is comparable to the calculated values of 0.13−7.7 per 1000 carbon atoms for this range of molecular weights, assuming a single saturated end for each chain. IR studies on high molecular weight samples of runs 1 and 8 indicate that vinyl unsaturation is observed for these high molecular weight unimodal polymers.

2.2.4. Aryl Ring Ligand Modification. The second part of the ligand to be modified was the aryl ring (Ar) attached to the imino nitrogens. Fe-based ketimine precatalysts **9**−**13** reveal that a reduction of steric bulk at the *ortho*-aryl position results in increases in activity and decreases in M_w. Fe precatalyst **9** contains isopropyl groups in the ortho positions of the aryl rings (Table 2, run 1) and displays a productivity of 5340 g/mmol·h·bar, approximately half that of *ortho*-dimethyl aryl derivative **10** (9340 g/mmol·h·bar, Table 2, run 2). The M_w drops from 611 000 to 242 000 on changing from *ortho*-isopropyl to *ortho*-methyl aryl groups. The replacement of one ortho group with a bulky *tert*-butyl group and the other ortho group with a proton (precatalyst **13**, Table 2, run 5) yields intermediate values of productivity and M_w. Replacing the *para*-aryl proton with a methyl group results in an increase in productivity from 9340 to 20600 g/mmol·h·bar and a decrease in M_w from 242 000 to 148 000. In the case of the cobalt complexes **14**−**16**, it is observed that the *ortho*-diisopropyl derivative **14** is less productive and gives lower molecular weight polymers than either the *ortho*-mono-*tert*-butyl or the mesityl derivatives **15** and **16**.

Fe-based aldimine precatalysts **17**−**20** display trends similar to those of their ketimine analogues, although trends are less pronounced, due to extremely broad polydispersities in the polymer product. When the ortho positions are substituted with ethyl and isopropyl groups (Table 2, runs 11,9), productivities of 305 (**17**) and 340 (**19**) g/mmol·h·bar are observed, with M_w's of 132 000 (**17**) and 230 000 (**19**). When smaller methyl groups are substituted (complex **18**), the productivity increases to 560 g/mmol·h·bar, and M_w decreases slightly to 108 000. Substitution of the para position with a methyl group has no apparent effect on the aldimine-derived catalysts.

2.2.5. Effect of Halide Group Variation. To examine the effect of the halide substituent on the precatalyst in the polymerization, we prepared two complexes, **11** and **12**, with identical metal centers and bis(imino)pyridine ligands but with chloride (**11**) and bromide (**12**) substituents. The productivity of the dichloride precatalyst **11** (20 600 g/mmol·h·bar) is slightly higher than the dibromide **12** (17 550 g/mmol·h·bar). The two precatalysts (Table 2; runs 3 and 4) afford polymers with similar properties.

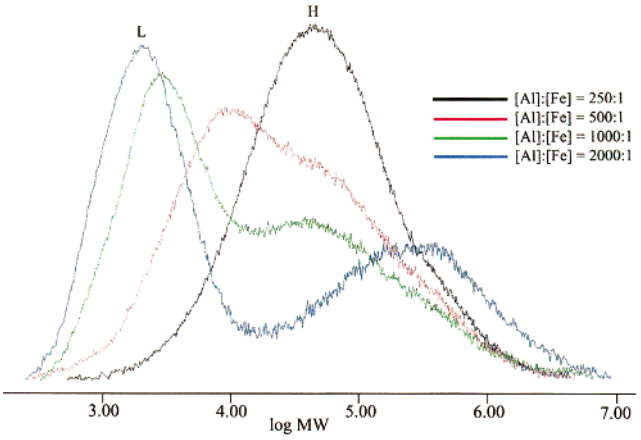

Figure 5. Effect of change in MAO concentration on the molecular weight distribution using precatalyst **9**.

2.2.6. Effect of Reaction Conditions on Polymer Product. The conditions of the polymerization reaction influence the productivity of the catalyst system employed and the nature of the polymer produced. To study these effects, we undertook a series of experiments under various conditions, employing Fe and Co ketimine precatalysts **9**, **11**, and **14**.

(i) Effect of MAO. To examine the role of the cocatalyst in the polymerization, we carried out several tests in which the ratio of [MAO]/[Fe] was systematically varied from 250:1 to 2000:1. Figure 5 shows a series of GPC traces for four polymerization tests of precatalyst **9** at 25 °C, 1 bar ethylene; Table 3 lists the results.

At 250 equiv of MAO (Figure 5, trace 1) a broad unimodal molecular weight distribution is observed, centered at 36 000 (M_{pk}). As the ratio of [MAO]/[Fe] is increased to 500:1 (Figure 5, trace in red), a broader distribution is observed, with a M_{pk} at 8500 and a shoulder at around 35 000. At 1000 equiv the distribution has become clearly bimodal, with a lower molecular weight fraction centered at 2800 and a higher molecular weight fraction at 46 000. At 2000 equiv of MAO (Figure 5, trace 4), the lower molecular weight peak is most prominent, accounting for 70% of the sample, and the two fractions have drifted further apart (2000 and 432 000, respectively.). These results parallel the effects observed by Brookhart and Small, using MMAO as cocatalyst.[19]

Toluene Soxhlet extraction over 3 days of the bimodal product obtained using 2000 equiv of MAO resulted in clean separation of the two fractions. Analysis of the PE end groups by ^{1}H NMR spectroscopy clearly showed that the lower molecular fraction is essentially saturated (17.6 saturated end groups/1000 C versus 0.25 vinyl end groups/1000 C); end group analysis of the higher molecular weight fraction is inherently more difficult due to the low solubility of this material, but the presence of vinyl end groups is indicated by ^{1}H NMR and IR spectroscopy.

(ii) Effect of Reaction Time. The reaction time can have a significant effect on productivity, molecular weight distribution, and the polymer end groups as exemplified for Fe precatalyst **11**. As reaction time increases from 12 to 60 min, the proportion of low molecular weight polymer decreases from 8% to 2%, and the position of the high molecular weight peak

(29) Haslam, J.; Willis, H. A.; Squirrel, D. C. M. *Identification and Analysis of Plastic*, 2nd ed.; Iliffe Books: London, U.K., 1972.

Table 3. Effect of Changes in [MAO] on the Bimodality of Polymer Employing Precatalyst **9**[a]

[MAO]/[Fe]	yield (g)	activity (g/mmol·h·bar)	M_w	M_n	M_w/M_n	M_{pk} peak 1 (%)	M_{pk} peak 2 (%)
250:1	0.66	2640	140000	22000	6.5		36000 (100)
500:1	1.11	4400	111000	7800	14.3		8500 (100)
1000:1	1.54	6160	113000	3900	29.3	2800 (50)	46000 (50)
2000:1	1.03	4120	245000	2700	90.7	2000 (70)	432000 (30)

[a] [Fe] = 0.5 μmol, 1 bar ethylene pressure, toluene solvent, RT, reaction time 1 h.

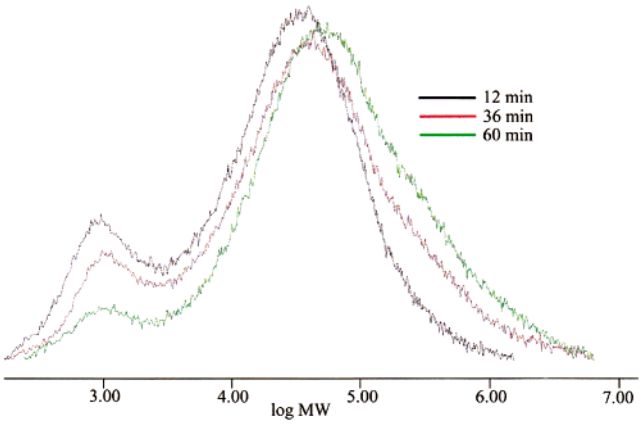

Figure 6. Effect of reaction time on bimodality of polymer employing precatalyst **9**.

Table 4. Effect of Reaction Time on the Bimodality of the Polymer Employing Procatalyst **11**[a]

reaction time (min)	yield (g)	activity (g/mmol·h·bar)	M_n	M_w	M_w/M_n	M_{pk} peak 1 (%)	M_{pk} peak 2 (%)
12	20.5	44890	3600	53000	14.8	1000 (8)	31000 (92)
36	32.5	23700	5400	146000	26.8	1000 (4)	43000 (96)
60	36.6	16050	9400	208000	22.0	900 (2)	47000 (98)

[a] [Fe] = 0.57 μmol, 4 bar ethylene pressure, isobutane solvent, 50 °C, 100 equiv of MAO, triisobutylaluminum scavenger.

progressively shifts to slightly higher molecular weight, with a high molecular weight shoulder appearing (Figure 6 and Table 4). As the reaction time increases, the number of saturated chain ends (per 1000 carbon atoms) decreases from 1.9 to 1.1, the number of vinyl chain ends remains constant at approximately 0.7 per 1000 carbon atoms, and the number of isopropyl chain ends decreases from 1.0 to 0.6 per 1000 carbon atoms.

(iii) Variation in Ethylene Pressure. The ethylene pressure can have an effect on both the yield and the molecular weight distribution of the polymer. For example, employing precatalyst **9** at 1 bar ethylene with 2000 equiv of MAO, a polymer displaying a bimodal distribution (Figure 5, trace 4) is produced. On increasing the pressure to 4 bar a unimodal distribution is observed with the a peak centered at 23 000. A similar effect is observed using precatalyst **11**. Under conditions in which unimodal distributions of the molecular weight are observed, the yield of PE increases linearly with pressure for both iron and cobalt precatalysts while the activity of the catalyst and the molecular weight remain essentially invariant. Figures 7 and 8 show the linear dependence of yield on ethylene pressure using Fe precatalysts **9** and Co precatalysts **14**; Table 5 shows the effects on molecular weight (M_{pk}) and activity.

(iv) Effect of Temperature on Catalyst Performance. A series of experiments were undertaken to determine the effect of temperature variation on catalyst performance. Table 6 shows the results of polymerizations performed at three different

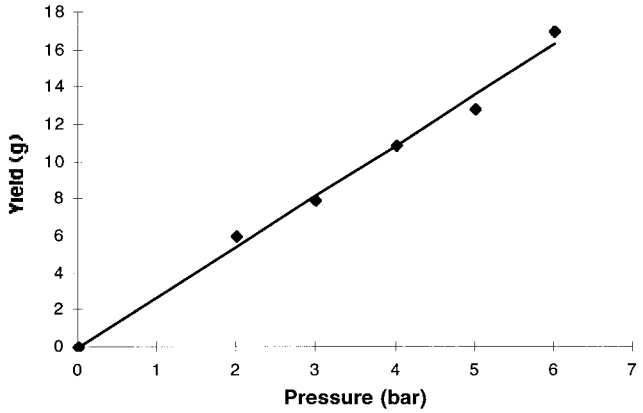

Figure 7. Effect of ethylene pressure on the yield of polymer employing iron precatalyst **9**.

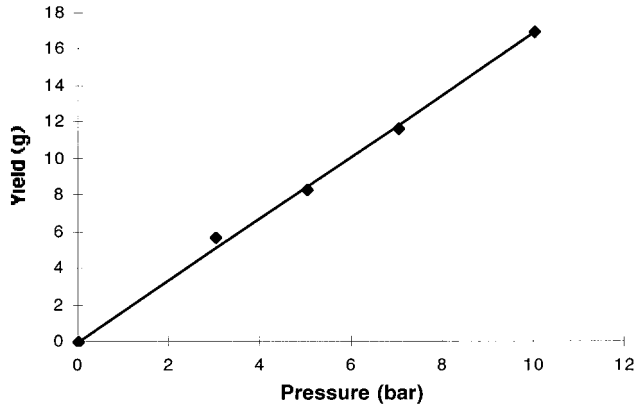

Figure 8. Effect of ethylene pressure on the yield of polymer employing cobalt precatalyst **14**.

Table 5. Effect of Ethylene Pressure on Precatalysts **9** and **14**[a]

procatalyst (μmol)	ethylene pressure (bar)	yield (g)	activity (g/mmol·h·bar)	M_{pk}
9 (0.57)	2	6.0	5260	232000
9 (0.57)	3	7.9	4600	216000
9 (0.57)	4	10.9	4780	285000
9 (0.57)	5	12.8	4490	329000
9 (0.57)	6	17.0	4980	304000
14 (7.4)	3	5.7	250	12000
14 (7.4)	5	8.3	230	14000
14 (7.4)	7	11.7	225	12000
14 (7.4)	10	17.0	230	12000

[a] Isobutane solvent, reaction time 1 h, 50 °C, 100 equiv of MAO, triisobutylaluminum scavenger.

temperatures (35, 50, and 70 °C), employing Fe precatalyst **9** and Co precatalyst **14**. In both cases, two effects are observed.

First, a significant reduction in the productivity of catalysts results [from 10 800 g/mmol·h·bar at 35 °C to 1140 g/mmol·h·bar at 70 °C (**9**); from 360 g/mmol·h·bar at 35 °C to 150 g/mmol·h·bar at 70 °C (**14**)], and second, the molecular weight (M_{pk}) of the polymer is considerably reduced [from 386 000 at

Table 6. Effect of Temperature on the Performance of Precatalysts **9** and **14**[a]

procatalyst (μmol)	temperature (°C)	yield (g)	activity (g/mmol·h·bar)	M_{pk}
9[b] (0.57)	35	12.3	10800	386000
9[b] (0.57)	50	6.0	5260	237000
9[b] (1.1)	70	2.6	1140	14000
14[c] (7.4)	35	26.1	360	16000
14[c] (7.4)	50	17.0	230	12000
14[c] (7.4)	70	11.4	150	8800

[a] Isobutane solvent, reaction time 1 h, 100 equiv of MAO, triisobutylaluminum scavenger. [b] Two bars of ethylene. [c] Ten bars of ethylene.

35 °C to 14 000 at 70 °C (**9**); from 16 000 at 35 °C to 8800 at 70 °C (**14**)].

2.3. Analysis of Decomposition Products of Activated Catalysts. To determine whether alkylaluminum species in MAO react with 2,6-bis(imino)pyridines ligands during polymerization to yield alternative active species, complex **9** was examined following activation with MAO and polymerization of ethylene. At several concentrations of MAO, **9** was stirred at 50 °C in toluene for 1 h or exposed to ethylene (1 bar) for 10 min at room temperature. The reaction was quenched by addition of dilute HCl, and the organic layer filtered and extracted. Analysis by NMR spectroscopy revealed that only the intact 2,6-bis(imino)pyridyl ligand (**1**) was recovered. There was no evidence for nucleophilic attack at the imine functionality by a methyl anion. In a separate study, we have shown that trimethylaluminum can react with 2,6-bis(imino)pyridines to give an aluminum complex containing the pyridyliminoamide moiety, but such attack only occurs on the free 2,6-bis(imino)-pyridine molecule and only at temperatures in excess of 80 °C.[30]

3. Discussion

3.1. General. The design of the Fe and Co catalyst systems described in this report is based on the observation that a 14-electron alkyl cation is commonly postulated as the active species for α-olefin polymerization.[2,17] Here, we sought to produce an active cationic 14-electron alkyl species through the use of a Group 8 metal with a neutral tridentate ligand, such as the bis(imino)pyridine ligand. Because bis-chelation was observed for sterically undemanding 2,6-bis(imino)pyridine ligands,[31−38] we chose to use ligands with bulky substituents on the imino nitrogen donors. Aryl groups with substituents in the ortho position produced the desired mono-chelation and an active ethylene polymerization catalyst. Related mono-chelated complexes have been reported for Mn,[39] Co,[40] Ru,[41] and Rh.[42−44]

3.2. Ligand Synthesis and Characterization. The relative ease of synthesis of both the ligands, 2,6-$(ArNCR^1)_2C_5H_3N$, and the final metal halide complexes, $\{2,6\text{-}(ArNCR^1)_2C_5H_3N\}MX_n$, made precatalyst modification relatively straightforward (Scheme 1). In particular, we sought to modify four aspects of the precatalyst: aryl ring-substituents, imino-substituents, halide group, and metal center.

Substituents on the aryl ring were introduced through use of the corresponding aniline in the condensation reaction that yields the ligand. Ligands bearing ketimine (R^1 = Me) or aldimine (R^1 = H) functionalities on the backbone were produced by variation of the 2,6-dicarbonylpyridine starting material from 2,6-diacetylpyridine to 2,6-pyridinedicarboxaldehyde. Use of the appropriate metal halide yielded complexes with metal centers of Fe and Co and ancillary chloride and bromide ligands.

Single-crystal X-ray diffraction analyses of Fe complexes **9**, **11**, and **12** and the Co complex **14** display similar coordination spheres (Figures 1 and 2). Indeed, identical solid-state structures are observed for the isomorphous pairs **9**,**14** and **11**,**12**. Significant differences between the isomorphous pairs, that is, the square pyramidal geometry for **9**,**14** and the trigonal pyramidal geometry for **11**,**12** can be seen in the side-on view shown in Figure 3. The origin of these structural differences is uncertain, but clearly, it demonstrates a certain degree of flexibility in the metal coordination geometry, which may be important for subsequent catalysis.

Since Fe is a group 8 metal and Co a group 9 metal, it is expected that the electronic environments will differ between their complexes. This is confirmed by measurement of magnetic moments, which show the Fe(II) complexes (**9**−**13**, **17**−**20**) to possess four unpaired electrons (quintet multiplicity, $2S + 1 = 5$) and Co(II) complexes (**14**−**16**, **21**) to have three unpaired electrons (quartet multiplicity, $2S+1 = 4$).[24,25] In addition the ^{1}H NMR spectra of the isostructural iron and cobalt complexes **9** and **14** show different chemical shifts for the corresponding protons (Figure 4).

A common feature of the Fe(II) complexes, **9**−**13** and **17**−**20**, is that they are all intensely colored. The origin of the strong colors is uncertain, and examples of spectroscopically characterized five-coordinate Fe(II) complexes bound by mono-chelating tridentate ligands are rare.[45] The strong absorption displayed in the UV−vis spectra of all the Fe(II) complexes at ∼700 nm, although uncertain, would seem attributable to metal to ligand charge transfer (MLCT). Further studies are underway to elucidate the orbital origin of this transition.

3.3. Ethylene Polymerization. Upon activation with MAO, all Fe and Co complexes **9**−**22** studied here are highly active ethylene polymerization catalysts. All of the catalysts convert ethylene to highly linear polyethylene, which is in contrast to the branching observed using Ni(II)- and Pd(II)-α-diimine catalysts.[10−14] Observations to date indicate that these systems are limited in their ability to incorporate higher α-olefins into growing polymer chains, which is also consistent with the lower productivities reported for the polymerization of propylene.[46−48]

(30) Bruce, M. D.; Gibson, V. C.; Redshaw, C.; Solan, G. A.; White, A. J. P.; Williams, D. J. *Chem. Commun.* **1998**, 2523−2524.
(31) Krumholz, P. *Inorg. Chem.* **1965**, *4*, 612−616.
(32) Curry, J. D.; Robinson, M. A.; Busch, D. H. *Inorg. Chem.* **1967**, *6*, 1570−1574.
(33) Blandamer, M. J.; Burgess, J.; Haines, R. I.; Mekhail, F. M.; Askalani, P. *J. Chem. Soc., Dalton Trans.* **1978**, 1001−1008.
(34) Stoufer, R. C.; Busch, D. H. *J. Am. Chem. Soc.* **1956**, *78*, 6016−6019.
(35) Figgins, P. E.; Busch, D. H. *J. Am. Chem. Soc.* **1960**, *82*, 820−824.
(36) Lions, F.; Martin, K. V. *J. Am. Chem. Soc.* **1957**, *79*, 2733−2738.
(37) Onggo, D.; Craig, D. C.; Rae, D.; Goodwin, H. A. *Aust. J. Chem.* **1991**, *44*, 331−341.
(38) Scheer, C.; Chautemps, P.; Gautier-Luneau, I.; Pierre, J.-L.; Serratrice, G.; Saint-Aman, E. *Polyhedron* **1996**, *15*, 219−224.
(39) Edwards, D. A.; Mahon, M. F.; Martin, W. R.; Molloy, K. C.; Fanwick, P. E.; Walton, R. A. *J. Chem. Soc., Dalton Trans.* **1990**, 3161−3168.
(40) Edwards, D. A.; Edwards, S. D.; Martin, W. R.; Pringle, T. J.; Thornton, P. *Polyhedron* **1992**, *11*, 1569−1573.
(41) Çetinkaya, B.; Çetinkaya, E.; Brookhart, M.; White, P. S. *J. Mol. Catal. A: Chem.* **1999**, *142*, 101−112.
(42) Haarman, H. F.; Ernsting, J. M.; Kranenburg, M.; Kooijman, H.; Veldman, N.; Spek, A. L.; van Leeuwen, P. W. N. M.; Vrieze, K. *Organometallics* **1997**, *16*, 887−900.
(43) Haarman, H. F.; Bregman, F. R.; Ernsting, J. M.; Veldman, N.; Spek, A. L.; Vrieze, K. *Organometallics* **1997**, *16*, 54−67.
(44) Haarman, H. F.; Bregman, F. R.; van Leeuwen, P. W. N. M.; Vrieze, K. *Organometallics* **1997**, *16*, 979−985.
(45) Morassi, R.; Bertini, I.; Sacconi, L. *Coord. Chem. Rev.* **1973**, 343−402.
(46) Small, B. L.; Brookhart, M. *Macromolecules* **1999**, *32*, 2120−2130.
(47) Brookhart, M. S.; Small, B. L. (DuPont/UNC), WO 98/30612, **1998** [*Chem. Abstr.* **1998**, *129*, 149375r].

Scheme 2. Possible Chain Propagation and Transfer Pathways

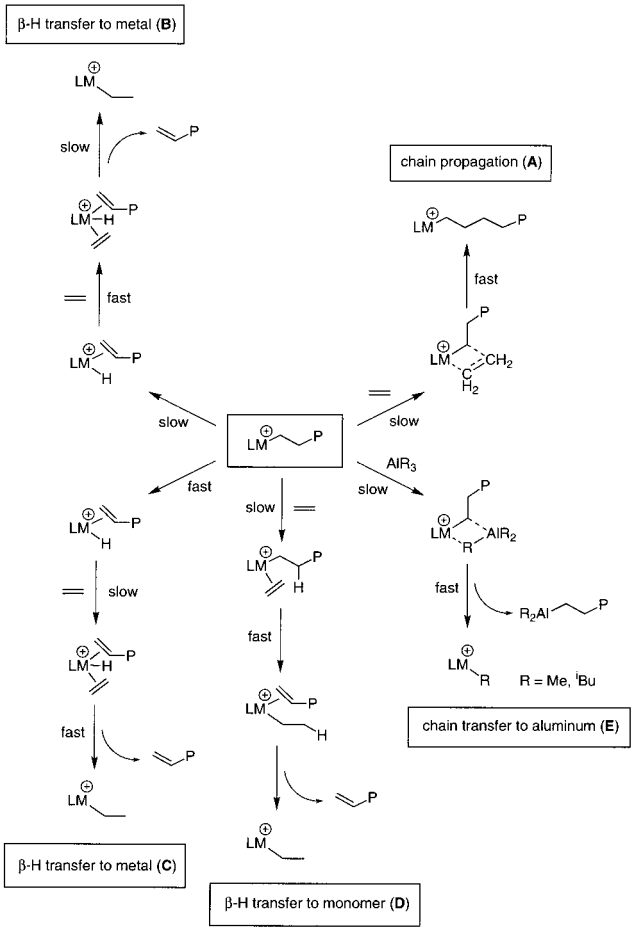

In this study, we have examined the effects of variations of the precatalyst as well as the reaction conditions on catalyst activity and polymer properties. Before we discuss these aspects in more detail, a general outline of the polymerization mechanism, that is, the propagation and chain-transfer pathways involved, would be helpful, since it forms the basis of the subsequent discussion (see Scheme 2). A Cossee-type propagation mechanism[49] (pathway **A**, Scheme 2) is assumed, involving migratory insertion of ethylene into a metal alkyl bond, whereby the rate has a first-order dependence upon the ethylene concentration (i.e., pressure). Four different chain-transfer pathways can be distinguished (Scheme 2). Two involve kinetically distinct β-H transfer to metal processes (**B** and **C**), a third β-H transfer to monomer (**D**), and a fourth chain transfer to aluminum (**E**). β-H transfer to metal of type **B** is a common chain-transfer process, especially for late transition metal catalysts. This β-H elimination reaction is unimolecular, that is, independent of monomer concentration, provided that the subsequent step, the associative displacement of the polymer chain by monomer, is fast and therefore is not the rate-determining step. If this is not the case, this chain-transfer process becomes a β-H transfer to metal of type **C**, which is kinetically indistinguishable from β-H transfer to monomer (**D**). These chain-transfer pathways are both bimolecular, that is, first order in monomer, and the latter (**D**) has been postulated previously for certain metallocene catalysts.[50−52] The fourth, less common chain-transfer reaction is chain transfer to aluminum (**E**). This process has also been observed for Ziegler−Natta systems,[53] Group 4 metallocenes,[51,54−59] and lanthanocenes[60,61] and is dependent upon the alkyl aluminum concentration. Scheme 2 shows a likely pathway involving formation of an alkyl-bridged Fe−Al species, which allows the growing polymer chain to be exchanged for a new alkyl group. Although this type of chain transfer might be expected to be zero order in ethylene, the possibility of a first-order dependence here cannot be ruled out, since a vacant site is still available at the iron center. It has not proved possible to draw a firm conclusion since a system is not available that undergoes chain transfer to aluminum exclusively. In general, β-H-transfer reactions, to the metal (**B** and **C**) or the monomer (**D**), give one unsaturated chain end per polymer chain (vinyl end groups), whereas chain transfer to aluminum (**E**) results in fully saturated polymer chains.

3.3.1 Precatalyst Modification. The first structural variable to be explored was the nature of the metal center. Fe-based precatalysts are more productive and afford higher molecular weight polymers to the corresponding Co systems. Fe-based precatalysts also exhibit different chain-transfer mechanisms than the corresponding Co systems. NMR analysis of Fe-produced polymers reveal both excess saturated chain ends and incorporation of isopropyl end groups, indicating that chain transfer in Fe systems involves a combination of β-H transfer and chain transfer to aluminum (isopropyl end groups are presumed to arise from triisobutylaluminum scavenger in the reactor). In contrast, all Co polymers, produced at low ethylene pressure (1 bar) and a large excess of MAO (2000 equiv), exhibit a 1:1 ratio of saturated to unsaturated ends, characteristic of chain transfer exclusively by β-H transfer. In light of the similarity of the solid-state structures for these systems, it is unlikely that the differences in the behavior of the Fe and Co precatalysts are due to steric effects. It would seem probable that the different inherent electronic properties of Fe and Co play an important role, possibly leading to the observed changes in the propagation and chain-transfer rates followed by the two systems.

The Fe(III) precatalyst **22** shows a similar activity compared to its Fe(II) analogue **20**. Also the polymer properties observed for both catalysts are rather similar, suggesting that the same active species is generated from both precatalysts. In this context, reduction of Fe(III) to Fe(II) species by alkyl aluminum compounds is not uncommon.[62]

The ligand environment around the metal center has a profound effect on catalyst productivity and molecular weight. Changing the ligand environment from a ketimine (R^1 = Me) to an aldimine (R^1 = H) results generally both in a large drop

(48) Pellecchia, C.; Mazzeo, M.; Pappalardo, D. *Macromol. Rapid Commun.* **1998**, *19*, 651−655.
(49) Cossee, P. *J. Catal.* **1964**, *3*, 80−88.
(50) Stehling, U.; Diebold, J.; Kirsten, R.; Röll, W.; Brintzinger, H.-H.; Jüngling, S.; Mülhaupt, R.; Langhauser, F. *Organometallics* **1994**, *13*, 964−970.
(51) Busico, V.; Cipullo, R. *Macromolecules* **1994**, *27*, 7538−7543.
(52) Tsutsui, T.; Mizuno, A.; Kashiwa, N. *Polymer* **1989**, *30*, 428−431.
(53) Marques, M. M. V.; Nunes, C. P.; Tait, P. J. T.; Dias, A. R. *J. Polym. Sci. A* **1993**, *31*, 219−225.
(54) Siedle, A. R.; Newmark, R. A.; Schroepfer, J. N.; Lyon, P. A. *Organometallics* **1991**, *10*, 400−404.
(55) Bochmann, M.; Lancaster, S. J. *Angew. Chem., Int. Ed. Engl.* **1994**, *33*, 1634−1637.
(56) Zambelli, A.; Longo, P.; Grassi, A. *Macromolecules* **1989**, *22*, 2186−2189.
(57) Soga, K.; Kaminaka, M. *Makromol. Chem.* **1993**, *194*, 1745−1755.
(58) Naga, N.; Mizunuma, K. *Polymer* **1998**, *39*, 5059−5067.
(59) Chien, J. C. W.; Wang, B.-P. *J. Polym. Sci. A* **1990**, *28*, 15−38.
(60) Pelletier, J. F.; Mortreux, A.; Petit, F.; Olonde, X.; Bujadoux, K. *Stud. Surf. Sci. Catal.* **1994**, *89*, 249−256.
(61) Pelletier, J. F.; Mortreux, A.; Olonde, X.; Bujadoux, K. *Angew. Chem., Int. Ed. Engl.* **1996**, *35*, 1854−1856.
(62) Yamamoto, A.; Morifuji, K.; Ikeda, S.; Saito, T.; Uchida, Y.; Misono, A. *J. Am. Chem. Soc.* **1968**, *90*, 1878−1883.

in productivity and in a decrease in the molecular weight. These results suggest that, for aldimine catalysts, the rate of propagation is decreased more than the rate of β-H transfer (the major chain-transfer process), resulting in lower productivites and lower molecular weights. Both Fe-based ketimine and aldimine precatalysts terminate by a combination of chain transfer to aluminum and β-H transfer, as shown by the ratio of saturated/unsaturated end groups being greater than 1 and the incorporation of isopropyl groups (from Al*i*-Bu_3 scavenger) observed for the ketimine-based catalysts. The observed differences between ketimine and aldimine systems is most likely related to the freedom of rotation of the aryl ring substituents.[46]

Changing the ancillary halide from Br (**12**) to Cl (**11**) results in a slight increase in activity but yields polymers exhibiting comparable molecular weight and similar numbers of saturated and unsaturated end groups. This suggests that identical active species are responsible for the polymerization.

Changes in the substituents on the aryl ring influence productivity but have more important consequences with respect to molecular weight. Ketimine-based systems show some clear trends, while trends in aldimine-based systems are less pronounced, due to extremely large polydispersities. From these results, it can be concluded that an increase in steric bulk in the ortho position results in a reduction of the rate of β-H transfer, giving higher molecular weight polyethylene. It is important to note here that, in reports by us and by Brookhart and co-workers, one single small ortho substituent leads to oligomerization rather than polymerization catalysts.[22,63]

3.3.2. Reaction Conditions. An interesting aspect of these systems is that polymerization tests on a particular catalyst under one set of conditions give a bimodal molecular weight distribution, yet for the same catalyst under slightly different conditions, a broad unimodal molecular weight distribution is obtained. Bimodal molecular weight distributions indicate that two processes are occurring. These processes may occur either consecutively or concurrently, and there are therefore two likely explanations to account for bimodality. First, there may be two active sites operating at the same time, and second, the mode of catalyst propagation and chain transfer may change during the course of polymerization.

The first possible explanation for a bimodal molecular weight distribution is that the polymer produced may be the result of two independent species. A starting point for studies into this possibility is the idea that the methyl groups in MAO react with the imine functionality in the ligand system to give another active species.[30] Analysis of the decomposition post-polymerization products does not confirm this; all that is recovered are the original ligand systems. One explanation as to why this does not occur during the polymerization of **9** could be due to the stability of the iron complex. For methyl migration to occur, the aluminum would have to displace the ligand from the iron complex to form an adduct with trimethylaluminum (in MAO).

A second, more likely explanation for bimodal molecular weight distributions is that different polymerization mechanisms are operating during polymerization. To explore this possibility, we undertook a series of experiments in which the reaction conditions were varied.

The first variable explored was the relative ratio of cocatalyst to precatalyst, which leads to three effects. First, increasing the MAO concentration results in higher productivities. This effect is most likely due to an increase in the number of active sites. Second, a greater proportion of MAO leads to a more pronounced bimodal molecular weight distribution, in particular to a sharp increase in the ratio of the low (L)/high (H) molecular weight fractions, as shown in Figure 5. The bimodal product that was obtained using 2000 equiv of MAO was fractionated via Soxhlet extraction with toluene and end group analysis by ^{1}H NMR shows that the lower molecular weight fraction is almost fully saturated (17.6 saturated end groups/1000 C versus 0.25 vinyl end groups/1000 C), indicating that chain transfer to aluminum is responsible for this low molecular weight product. To explain this observation, we have to consider that an increase in the MAO concentration will cause an increase in the rate of chain transfer to aluminum, possibly exceeding the rate of β-H transfer for some time during the polymerization, resulting in an increase in the proportion of the lower molecular weight fraction (L). Additionally, higher MAO concentrations lead to a significant shift of fraction L to lower molecular weights. An increase in the MAO concentration will enhance the rate of chain transfer to aluminum which, combined with a constant rate of propagation, will result in even shorter polymer chains. A graphical illustration of this is shown in Figure 9, wherein panel a is representative of a low MAO concentration regime and panel b is the higher MAO concentration regime.

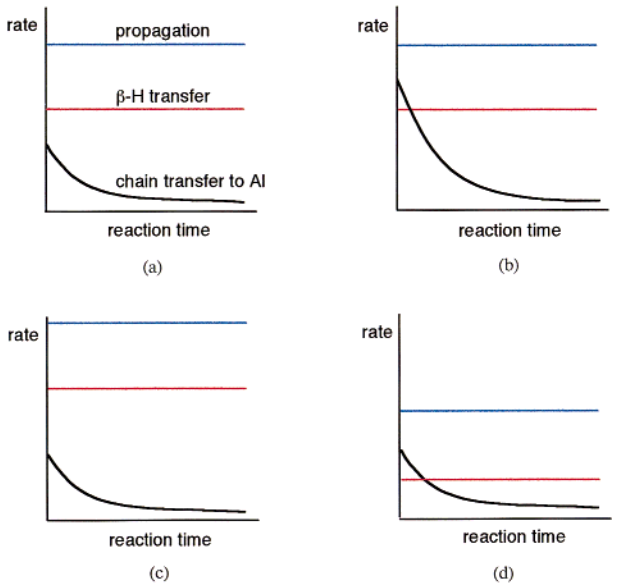

Figure 9. Schematic representations of the effects of different reaction conditions on the rates of propagation and chain termination: (a) low MAO concentration, (b) high MAO concentration, (c) high pressure, (d) low pressure.

Studies on the effect of reaction time reveal that at short time intervals higher ratios of the low/high molecular weight fraction and higher ratios of saturated/unsaturated end groups are found. These observations imply that the low molecular weight portion of the polymer, consisting of mostly saturated chains, is actually created early on in the course of the polymerization reaction. The rate of the chain transfer to aluminum will be highest at the beginning of the polymerization, when the Al concentration is at its peak (see Figure 9b). As the polymerization reaction proceeds, depletion of the available alkylaluminum as a result of this chain-transfer reaction will decrease the rate of chain transfer to aluminum, while the rate of β-H transfer will remain constant as it is only dependent upon the concentration of monomer. Consequently, at longer times this transfer process becomes dominant, giving vinyl terminated higher molecular weight products. Additionally, with time, the rate of chain transfer to aluminum may also decrease as the catalyst becomes

(63) Small, B. L.; Brookhart, M. *J. Am. Chem. Soc.* **1998**, *120*, 7143−7144.

increasingly embedded in the polymer (diffusion-controlled chain transfer).

These conclusions are supported by studies on variations in reaction pressure, a third parameter that affects bimodality. A series of experiments in which the pressure of ethylene was increased revealed that, for both Fe and Co systems (**9** and **14**, respectively), the yield of polyethylene increased but the molecular weight did not (Figures 7 and 8, Table 5). The increase in yield is linear and demonstrates that the rate of propagation has a first-order rate dependence on ethylene, in accordance with the proposed Cossee-type mechanism.[49] The fact that molecular weight remained constant indicates that the overall rate of chain transfer must also be first order in ethylene. This result implies that β-H transfer to the metal (pathway **B** in Scheme 2) is not operating as the product-determining chain-transfer process, since zero-order dependence on monomer concentration would be expected. Low molecular weight peaks account for ~10% of the polymer under the conditions used in these experiments. Thus, assuming that only the low molecular weight portion is subject to chain transfer to aluminum, one will observe a rate equation consistent with β-H transfer (**C** or **D**) as the predominant chain-transfer process. An increase in pressure results in a decrease in the proportion of low molecular weight product. This can be explained by considering that increasing the pressure will result in an increase in the rate of propagation and also the rate of the β-H-transfer process but not the rate of chain transfer to aluminum (Figure 9c). At higher pressures β-H transfer will become the dominant chain-transfer process, giving mainly vinyl terminated high molecular weight polymer. As the pressure is lowered, the rate of β-H transfer will be reduced and chain transfer to aluminum can become competitive or even dominant (Figure 9d). The change in the ratio of low/high molecular weight product with pressure seems to indicate that the chain transfer to aluminum is not ethylene pressure-dependent, although some degree of diffusion control cannot be ruled out.

Experiments in which the temperature of the polymerization reaction was varied reveal that an increase in temperature results in large decreases in productivity and molecular weight. Elevated temperatures will result in higher propagation and chain-transfer rates, which would be expected to afford higher productivities and lower molecular weight products. However, there are two counter effects to this that are likely to be operating. First, a decrease in ethylene solubility at higher temperatures[64,65] (i.e., lower monomer concentrations) will lead to reduced productivity, and second, higher temperatures can result in higher rates of catalyst deactivation. It is a combination of these effects that is likely to account for the observed temperature dependence.

4. Conclusions

The synthesis and characterization of a new family of iron- and cobalt-based ethylene polymerization precatalysts have been described. Activation with MAO produces highly active catalysts; ketimine-based catalysts are more active than aldimine-based systems, and Fe is an order of magnitude more active than Co. These catalyst systems produce polymers with a wide range of molecular weights, depending on the metal center and the 2,6-bis(imino)pyridyl ligand; steric bulk in the ortho position of the aryl rings appears to be of critical importance. Two chain-transfer pathways have been identified: β-H transfer (to monomer or metal) and chain transfer to aluminum. The ratio between the rates of these two chain-transfer processes and the rate of propagation is influenced not only through modifications to the catalyst but also by changes in reaction conditions, allowing the resultant molecular weight distribution to be systematically altered. Work is underway to understand more fully the nature of the active site in these systems and, in particular, the role and influence of the ligand substituents, which will allow further rational modification of these catalysts.

5. Experimental Section

5.1. General. All manipulations were carried out under an atmosphere of nitrogen using standard Schlenk and cannula techniques or in a conventional nitrogen-filled glovebox. Solvents were refluxed over an appropriate drying agent and distilled and degassed prior to use. Elemental analyses were performed by the microanalytical services of the Department of Chemistry at Imperial College and Medac Ltd. NMR spectra were recorded on a Bruker spectrometer at 250 MHz (^{1}H) and 62.9 MHz (^{13}C) at 293 K; chemical shifts are referenced to the residual protio impurity of the deuterated solvent. Mass spectra were obtained using either fast atom bombardment (FAB), electron impact (EI), or chemical ionization (CI). Gel permeation chromatographs (GPCs) were obtained using a Waters 150CV (columns supplied by Shodex (807, 806, & 804)) (BP Chemicals Ltd.) at 135 °C. IR spectra of the polymers were recorded on a Nicolet 730 FTIR spectrometer. Magnetic Susceptibility studies were performed using and Evans balance or by using the Evans NMR method (solvent, CD_2Cl_2; reference, cyclohexane).[24,25]

Compound 2,6-pyridinedicarboxaldehyde was prepared according to an established procedure,[66] while 2,6-diacetylpyridine, MAO (10% solution in toluene), and all of the anilines were purchased from Aldrich Chemical Co. All other chemicals were obtained commercially and used as received unless stated otherwise.

5.2. Preparations of 2,6-Bis(imino)pyridyl Ligands. 5.2.1. 2,6-Diacetylpyridinebis(2,6-diisopropylanil) (1). To a solution of 2,6-diacetylpyridine (1.50 g, 9.2 mmol) in absolute ethanol (25 mL) was added 2,6-diisopropylaniline (3.46 mL, 18.4 mmol). After the addition of a few drops of glacial acetic acid, the solution was refluxed overnight. Upon cooling to room temperature, the product crystallized from ethanol. After filtration the yellow solid was washed with cold ethanol and dried in a vacuum oven (50 °C) overnight to give 3.54 g (80%) of **1**. ^{1}H NMR ($CDCl_3$): δ 8.52 (d, 2H, ^3J(HH) 7.8, Py-H_m), 7.94 (t, 1H, Py-H_p), 7.1 (m, 6H, Ar-*H*), 2.78 (sept, 4H, ^3J(HH) 5.6, C*H*Me$_2$), 2.28 (s, 6H, N=C*Me*), 1.18 (d, 24H, CH*Me*$_2$).^{13}C NMR ($CDCl_3$,^{1}H gated decoupled): δ 167.04 (N=*C*), 155.25 (Py-C_o), 146.25 (Ar-C_{ip}), 135.69 (Ar-C_o), 123.75 (Ar-C_p), 123.02 (Py-C_p), 122.57 (Py-C_m), 122.30 (Ar-C_m), 28.32 (N=C-*Me*), 23.21 (CH*Me*$_2$), 17.15 (*C*HMe$_2$). EI mass spectrum, *m*/*z* 481 [M^+]. Anal. ($C_{33}H_{43}N_3$) calcd: C, 82.32; H, 8.94; N, 8.73. Found: C, 82.11; H, 8.91; N, 8.69.

5.2.2. 2,6-Diacetylpyridinebis(2,6-dimethylanil) (2). By using the procedure described in (5.2.1) above, we obtained **2** as a yellow powder in 78% yield. ^{1}H NMR ($CDCl_3$): δ 8.48 (d, 2H, ^3J(HH) 7.8, Py-H_m), 8.13 (t, 1H, Py-H_p), 7.98, 7.08−6.5, (m, 6H, Ar-*H*), 2.25 (s, 6H, N=C*Me*), 2.05 (s, 12H, C*Me*). EI mass spectrum, *m*/*z* 369 [M^+]. Anal. ($C_{25}H_{27}N_3$) calcd: C, 81.30; H, 7.32; N, 11.38. Found: C, 81.11; H, 7.29; N, 11.32.

5.2.3. 2,6-Diacetylpyridinebis(2,4,6-trimethylanil) (3). By using the procedure described in (5.2.1) above, we obtained **3** as a yellow powder in 60% yield. ^{1}H NMR ($CDCl_3$): δ 8.50 (d, 2H, ^3J(HH) 7.9, Py-H_m), 7.95 (t, 1H, Py-H_p), 6.94 (s, 4H, Ar-*H*), 2.33 (s, 6H, N=C*Me*), 2.28 (s, 6H, C*Me*), 2.05 (s, 12H, C*Me*). ^{13}C NMR ($CDCl_3$,^{1}H gated decoupled): δ 167.43 (N=*C*), 155.06 (Py-C_o), 146.22 (Ar-C_{ip}), 136.81 (Ar-C_o), 132.21 (Ar-C_p), 128.60 (Py-C_p), 125.16 (Py-C_m), 122.20 (Ar-C_m), 20.76 (N=C-*Me*), 17.89 (Ar-*Me*$_p$), 16.41 (Ar-*Me*$_o$). CI mass spectrum, *m*/*z* 397 [M^+]. Anal. ($C_{27}H_{31}N_3$) calcd: C, 81.57; H, 7.86; N, 10.56. Found: C, 81.42; H, 7.80; N, 10.30.

5.2.4. 2,6-Diacetylpyridinebis(2-tert-butylanil) (4). By using the procedure described in (5.2.1) above, we obtained **4** as a yellow powder

(64) Atiqullah, M.; Hammawa, H.; Hamid, H. *Eur. Polym. J.* **1998**, *34*, 1511−1520.

(65) Fogg, P. G. T.; Gerrard, W. *Solubility of gases in liquids*; Wiley: West Sussex, England, 1991.

(66) Alcock, N. W.; Kingston, R. G.; Moore, P.; Pierpoint, C. *J. Chem. Soc., Dalton Trans.* **1984**, 1937−1943.

in 76% yield. ^{1}H NMR ($CDCl_3$): δ 8.42 (d, 2H, ^3J(HH) 7.8, Py-H_m), 7.94 (t, 1H, Py-H_p), 7.44, 7.21, 7.09, and 6.56 (m, 8H, Ar-*H*), 2.43 (s, 6H, N=C*Me*), 1.39 (s, 18H, C*Me*). ^{13}C NMR ($CDCl_3$,^{1}H gated decoupled): δ 165.32 (N=*C*), 155.61 (Py-C_o), 149.66 (Ar-C_{ip}), 139.77 (Ar-*C*), 136.86 (Ar-C_o), 126.41 (Py-C_m), 123.75, 122.26 and 119.75 (Ar-*C*), 29.61 (C*Me*), 16.88 (N=C-*Me*). EI mass spectrum, *m*/*z* 425 [M^+]. Anal. ($C_{29}H_{35}N_3$) calcd: C, 81.84; H, 8.29; N, 9.87. Found: C, 81.03; H, 8.29; N, 9.75.

5.2.5. 2,6-Diformylpyridinebis(2,6-diisopropylanil) (5). To a solution of 2,6-pyridinedicarboxaldehyde (0.101 g, 0.75 mmol) in absolute ethanol (20 mL), were successively added 2,6-diisopropylaniline (2.1 equiv, 1.57 mmol, 0.26 mL) and one drop of glacial acetic acid, and the resulting mixture was refluxed for 24 h. Upon cooling, yellow crystalline **5** was obtained in high yield (0.270 g, 80%). ^{1}H NMR ($CDCl_3$): δ 8.44 (s, 2H, N=C*H*), 8.40 (d, 2H, ^3J(HH) 7.6, Py-H_m), 8.00 (t, 1H, Py-H_p), 7.23 (m, 6H, Ar-*H*), 3.01 (sept, 4H, ^3J(HH) 6.9, C*H*Me$_2$), 1.21 (d, 24H, CH*Me*$_2$). ^{13}C NMR ($CDCl_3$,^{1}H gated decoupled): δ 162.70 (N=*C*), 154.43 (Py-C_o), 148.30 (Ar-C_{ip}), 137.14 (Ar-C_o), 124.54 (Ar-C_p), 123.05 (Py-C_p), 122.90 (Ar-C_m), 122.76 (Py-C_m), 28.00 (*C*HMe$_2$), 23.44 (CH*Me*$_2$). CI mass spectrum, *m*/*z* 454 [(*M*+H)$^+$]. Anal. ($C_{31}H_{39}N_3$) calcd: C, 82.07; H, 8.66; N, 9.26. Found: C, 82.02; H, 8.90; N, 9.54.

5.2.6. 2,6-Diformylpyridinebis(2,6-dimethylanil) (6). By using the procedure described in (5.2.5) above, we obtained **6** as a yellow powder in 82% yield. ^{1}H NMR ($CDCl_3$): δ 8.43 (s, 2H, N=C*H*), 8.40 (d, 2H, ^3J(HH) 7.6, Py-H_m), 8.00 (t, 1H, Py-H_p), 7.10 (d, 4H, ^3J(HH) 7.4, Ar-H_m), 6.99 (t, 2H, Ar-H_p), 2.20 (s, 12H, Ar-*Me*). ^{13}C NMR ($CDCl_3$,^{1}H gated decoupled): δ 163.16 (N=*C*), 154.45 (Py-C_o), 150.26 (Ar-C_{ip}), 137.32 (Ar-C_o), 128.16 (Py-C_p), 126.77 (Py-C_m), 124.16 (Ar-C_p), 122.69 (Ar-C_m), 18.31 (Ar-Me_o). CI mass spectrum, *m*/*z* 342 [(*M*+H)$^+$]. Anal. ($C_{23}H_{23}N_3$) calcd: C, 80.94; H, 6.74; N, 12.32. Found: C, 80.62; H, 6.44; N, 12.29.

5.2.7. 2,6-Diformylpyridinebis(2,6-diethylanil) (7). By using the procedure described in (5.2.5) above, we obtained **7** as a yellow powder in 75% yield. ^{1}H NMR ($CDCl_3$): δ 8.44 (s, 2H, N=C*H*), 8.40 (d, 2H, ^3J(HH) 7.6, Py-H_m), 8.00 (t, 1H, Py-H_p), 7.25 (m, 6H, Ar-*H*), 2.55 (q, 8H, ^3J(HH) 7.5, Ar−CH_2Me), 1.61 (t, 12H, Ar−CH$_2$*Me*). ^{13}C NMR ($CDCl_3$,^{1}H gated decoupled): δ 162.79 (N=*C*), 154.45 (Py-C_o), 149.52 (Ar-C_{ip}), 137.33 (Ar-C_o), 132.69 (Py-C_p), 126.27 (Py-C_m), 124.36 (Ar-C_p), 122.62 (Ar-C_m), 24.68 (*C*H$_2$Me), 14.58 (CH$_2$*Me*). CI mass spectrum, *m*/*z* 398 [(*M*+H)$^+$]. Anal. ($C_{27}H_{31}N_3$) calcd: C, 81.57; H, 7.86; N, 10.57. Found: C, 81.65; H, 7.69; N, 10.71.

5.2.8. 2,6-diformylpyridinebis(2,4,6-trimethylanil) (8). By using the procedure described in (5.2.5) above, we obtained **8** as a yellow powder in 80% yield. ^{1}H NMR ($CDCl_3$): δ 8.42 (s, 2H, N=C*H*), 8.40 (s, 2H, Py-H_m), 8.0 (t, 1H, ^3J(HH) 8, Py-H_p), 7.0 (s, 4H, Ar-*H*), 2.33 (s, 6H, Ar-Me_p), 2.19 (s, 12H, Ar-Me_o). ^{13}C NMR ($CDCl_3$,^{1}H gated decoupled): δ 163.14 (N=*C*), 154.57 (Py-C_o), 147.84 (Ar-C_{ip}), 137.24 (Ar-C_o), 133.52 (Ar-C_p), 128.86 (Py-C_p), 126.80, (Py-C_m) 122.57 (Ar-C_m), 20.79 (Ar-Me_p), 18.27 (Ar-Me_o). EI mass spectrum, *m*/*z* 369 [M^+]. Anal. ($C_{25}H_{27}N_3$) calcd: C, 81.30; H, 7.32; N, 11.38. Found: C, 81.69; H, 7.51; N, 11.11.

5.3. Complexation with MX_2 (M = Fe, Co; X = Cl, Br). 5.3.1. Preparation of (2,6-Diacetylpyridinebis(2,6-diisopropylanil))$FeCl_2$ (9). A suspension of **1** (0.92 g; 1.89 mmol) in *n*-butanol was added dropwise at 80 °C to a solution of $FeCl_2$ (0.24 g; 1.89 mmol) in *n*-butanol (20 mL) to yield a blue solution. After being stirred at 80 °C for 15 min, the reaction was allowed to cool to room temperature. The reaction volume was concentrated, and diethyl ether (30 mL) was added to precipitate the product as a blue powder, which was subsequently washed with diethyl ether (3 × 10 mL), filtered, and dried to afford 0.93 g (81%) of **9**. ^{1}H NMR (CD_2Cl_2, broad singlets are observed in each case): δ 81.7 (2H, Py-H_m), 81.1 (1H, Py-H_p), 14.9 (4H, Ar-H_m), −5.3 (12H, *i*-Pr-*Me*), −6.3 (12H, *i*-Pr-*Me*), −10.9 (2H, Ar-H_p), −22.4 (4H, *i*-Pr−C*H*), −37.1 (6H, N=C(*Me*)). FAB mass spectrum, *m*/*z* 607 [M^+], 572 [M^+-Cl], 482 [M^+-$FeCl_2$]. Anal. ($C_{33}H_{43}N_3FeCl_2\cdot0.5H_2O$) calcd: C, 64.19; H, 7.18; N, 6.80. Found: C, 64.19; H, 6.90; N, 6.70. μ_{eff} (Evans Balance): 5.34 BM.

5.3.2. Preparation of (2,6-Diacetylpyridinebis(2,6-dimethylanil))$FeCl_2$ (10). The procedure as above in (5.3.1) using **2** and $FeCl_2$ gave **10** as a blue powder in 78% yield. ^{1}H NMR (CD_2Cl_2, broad singlets are observed in each case): δ 86.2 (2H, Py-H_m), 39.6 (1H, Py-H_p), 16.3 (4H, Ar-H_m), 13.4 (12H, Ar-*Me*), −11.3 (2H, Ar-H_p), −17.0 (6H, N=C(*Me*)). FAB mass spectrum, *m*/*z* 496 [M^+], 461 [M^+-Cl], 425 [M^+-2Cl]. Anal. ($C_{25}H_{27}N_3FeCl_2$) calcd: C, 60.48; H, 5.44; N, 8.47. Found: C, 60.11; H, 5.10; N, 8.01. μ_{eff} (Evans Balance): 5.31 BM.

5.3.3. Preparation of (2,6-Diacetylpyridinebis(2,4,6-trimethylanil))$FeCl_2$ (11). The procedure as above in (5.3.1) using **3** and $FeCl_2$ gave **11** as a blue powder in 64% yield. ^{1}H NMR (CD_2Cl_2, broad singlets are observed in each case): δ 83.7 (2H, Py-H_m), 40.1 (1H, Py-H_p), 21.8 (6H, Ar-Me_p), 15.7 (4H, Ar-H_m), 13.0 (12H, Ar-Me_o), −21.3 (6H, N=C(*Me*)). FAB mass spectrum, *m*/*z* 523 [M^+], 488 [M^+-Cl], 453 [M^+-2Cl]. Anal. ($C_{27}H_{31}N_3FeCl_2\cdot1.5H_2O$) calcd: C, 58.82; H, 6.22; N, 7.62. Found: C, 58.63; H, 6.20; N, 6.88. μ_{eff} (Evans Balance): 5.25 BM.

5.3.4. Preparation of (2,6-Diacetylpyridinebis(2,4,6-trimethylanil))$FeBr_2$ (12). The procedure as above in (5.3.1) using **3** and $FeBr_2$ gave **12** as a blue powder in 61% yield. ^{1}H NMR (CD_2Cl_2, broad singlets are observed in each case): δ 80.4 (2H, Py-H_m), 39.7 (1H, Py-H_p), 22.3 (6H, Ar-Me_p), 15.6 (16H, Ar-H_m, Ar-Me_o), −18.5 (6H, N=C(*Me*)). FAB mass spectrum, *m*/*z* 613 [M^+], 533 [M^+-Br], 453 [M^+-2Br]. Anal. ($C_{27}H_{31}N_3FeBr_2$) calcd: C, 52.88; H, 5.10; N, 6.85. Found: C, 52.82; H, 5.42; N, 6.51. μ_{eff} (Evans Balance): 4.71 BM.

5.3.5. Preparation of (2,6-Diacetylpyridinebis(2-tert-butylanil))$FeCl_2$ (13). The procedure as above in (5.3.1) using **4** and $FeCl_2$ gave **13** as a blue powder in 85% yield. ^{1}H NMR (CD_2Cl_2, broad singlets are observed in each case): δ 78.7 (2H, Py-H_m), 68.15 (1H, Py-H_p), 17.0 (2H, Ar-*H*), 1.70 (2H, Ar-*H*), −2.32 (18H, C*Me*), −14.3 (2H, Ar-*H*), −24.1 (6H, NCCH_3), −45.2 (2H, Ar-*H*). FAB mass spectrum, *m*/*z* 551 [M^+], 516 [M^+-Cl], 426 [M^+-$FeCl_2$]. Anal. ($C_{29}H_{35}N_3FeCl_2$) calcd: C, 63.06; H, 6.39; N, 7.61. Found: C, 63.09; H, 6.69; N, 7.35. μ_{eff} (Evans NMR Method): 5.11 BM.

5.3.6. Preparation of (2,6-Diacetylpyridinebis(2,6-diisopropylanil))$CoCl_2$ (14). The procedure as above in (5.3.1) using **1** and $CoCl_2$ gave **14** as a light brown powder in 67% yield. ^{1}H NMR (CD_2Cl_2, broad singlets are observed in each case): δ 117.1 (2H, Py-H_m), 49.91 (1H, Py-H_p), 10.07 (4H, Ar-H_m), 4.56 (6H, N=CCH_3), −8.75 (2H, Ar-H_p), −17.51 (12H, *i*Pr-*Me*), −18.51 (12H, *i*Pr-*Me*), −84.36 (6H, *i*Pr−C*H*). FAB mass spectrum, *m*/*z* 575 [M^+-Cl]. μ_{eff} (Evans NMR Method): 4.55 BM.

5.3.7. Preparation of (2,6-Diacetylpyridinebis(2,4,6-trimethylanil))$CoCl_2$ (15). The procedure as above in (5.3.1) using **3** and $CoCl_2$ gave **15** as a green powder in 94% yield. The product was recrystalized from hot 1,1,2,2-tetrachloroethane to give green needles. ^{1}H NMR (CD_2Cl_2, broad singlets are observed in each case): δ 111.4 (2H, Py-H_m), 36.14 (1H, Py-H_p), 16.92 (6H, p−CH_3), 6.33 (4H, Ar-H_m), −0.65 (6H, N=C−CH_3), −26.83 (12H, o−CH_3). Anal. ($C_{27}H_{31}N_3CoCl_2\cdot0.5H_2O$) calcd: C, 60.46; H, 6.01; N, 7.83. Found: C, 60.58; H, 5.79; N, 7.79. μ_{eff} (Evans Balance): 4.55 BM.

5.3.8. Preparation of (2,6-Diacetylpyridinebis(2-tert-butylanil))$CoCl_2$ (16). The procedure as above in (5.3.1) using **4** and $CoCl_2$ gave **16** as a golden-brown powder in 83% yield. ^{1}H NMR (CD_2Cl_2, broad singlets are observed in each case): δ 111.8 (2H, Py-H_m), 50.4 (1H, Py-H_p), 12.6 (2H, Ar-*H*), 10.4 (6H, NCCH_3), 1.92 (2H, Ar-*H*), −11.7 (2H, Ar-*H*), −25.7 (18H, C*Me*), −85.4 (2H, Ar-*H*). FAB mass spectrum, *m*/*z* 519 [M^+-Cl], 484 [M^+-2Cl]. μ_{eff} (Evans NMR Method): 4.71 BM.

5.3.9. Preparation of (2,6-Diformylpyridinebis(2,6-diisopropylanil))$FeCl_2$ (17). A suspension of **5** (0.245 g, 0.55 mmol, 1 equiv) in *n*-butanol (10 mL) was added dropwise at 80 °C to a solution of $FeCl_2$ (0.070 g, 0.55 mmol) in *n*-butanol (40 mL) to yield a dark green solution. After being stirred for 15 min at 80 °C, the mixture was allowed to cool to room temperature and was then stirred for a further 12 h. The solvent volume was reduced to ∼1 mL and the reaction mixture washed with diethyl ether (3 × 40 mL) to yield a dark green powder of **17** (0.205 g, 65%). ^{1}H NMR (CD_2Cl_2, broad singlets are observed in each case): δ 61.5 (2H, Py-H_m), 16.8 (1H, Py-H_p), 14.1 (4H, Ar-H_m), 2.1 (2H, Ar-H_p), 1.4 (4H, *i*-Pr−C*H*), 0.6 (24H, *i*-Pr-*Me*), −5.5 (2H, N=C-*H*). FAB mass spectrum: *m*/*z* 576 [M^+], 544 [M^+-Cl], 454 [M^+-$FeCl_2$]. Anal. ($C_{31}H_{39}N_3FeCl_2\cdot H_2O$) calcd: C, 62.22; H, 6.91; N, 7.02. Found: C, 62.18; H, 6.73; N, 6.92. μ_{eff} (Evans Balance): 5.51 BM.

Table 7. Crystal Data, Data Collection, and Refinement Parameters for Complexes **9**, **11**, **12**, and **14**[a]

data	**9**	**11**	**12**	**14**
formula	$C_{33}H_{43}N_3Cl_2Fe$	$C_{27}H_{31}N_3Cl_2Fe$	$C_{27}H_{31}N_3Br_2Fe$	$C_{33}H_{43}N_3Cl_2Co$
solvent	$0.5H_2O$	MeCN	MeCN	$0.5H_2O$
formula weight	617.5	565.4	654.3	620.5
color, habit	blue platy needles	blue platy needles	blue prisms	orange platy prisms
crystal size/mm	$0.40 \times 0.20 \times 0.03$	$0.57 \times 0.13 \times 0.03$	$0.23 \times 0.17 \times 0.05$	$0.67 \times 0.47 \times 0.10$
crystal system	triclinic	monoclinic	monoclinic	triclinic
space group	$P\bar{1}$ (no. 2)	$P2_1/n$ (no. 14)	$P2_1/n$ (no. 14)	$P\bar{1}$ (no. 2)
cell dimensions				
a/Å	8.779(1)	14.569(2)	14.536(2)	8.748(1)
b/Å	9.876(1)	15.099(1)	15.273(3)	9.866(1)
c/Å	20.976(1)	14.554(2)	14.676(2)	20.970(3)
α/deg	83.70(1)	—	—	84.14(1)
β/deg	88.18(1)	113.14(1)	112.41(1)	88.23(1)
γ/deg	65.67(1)	—	—	65.68(1)
V/Å^3	1646.9(3)	2943.9(7)	3012.2(8)	1640.5(4)
Z	2	4	4	2
D_c/g cm^{-3}	1.245	1.276	1.443	1.256
F(000)	654	1184	1328	656
radiation used	Cu−Kα	Cu−Kα	Cu−Kα	Mo−Kα
μ/mm^{-1}	5.36	5.95	7.29	0.71
θ range/deg	2.1−60.0	4.4−60.0	3.6−60.0	2.3−25.0
no. of unique reflections				
measured	4878	4365	4467	5372
observed, $\|F_o\| > 4\sigma(\|F_o\|)$	3595	2535	2738	3713
absorption correction	Gaussian	semiempirical	empirical	semiempirical
max., min. transmission	0.84, 0.31	0.63, 0.38	0.73, 0.29	0.96, 0.77
no. of variables	362	326	326	361
R_1 [b]	0.061	0.069	0.059	0.051
wR_2 [c]	0.144	0.144	0.118	0.099
weighting factors a, b [d]	0.075, 0.566	0.067, 0.000	0.043, 0.000	0.042, 0.000
largest diff. peak, hole/eÅ^{-3}	0.35, −0.48	0.30, −0.48	0.41, −0.41	0.37, −0.21

[a] Details in common: graphite monochromated radiation, ω-scans, Siemens P4/PC diffractometer, 293 K, refinement based on F^2. [b] $R_1 = \sum||F_o| - |F_c||/\sum|F_o|$. [c] $wR_2 = [\sum w(F_o^2 - F_c^2)^2/\sum w(F_o^2)^2]^{1/2}$. [d] $w^{-1} = \sigma^2(F_o^2) + (aP)^2 + bP$.

5.3.10. Preparation of (2,6-Diformylpyridinebis(2,6-dimethylanil))$FeCl_2$ (18). The procedure as above in (5.3.9) using **6** and $FeCl_2$ gave **17** as a green powder in 60% yield. ^{1}H NMR (CD_2Cl_2, broad singlets are observed in each case): δ 66.2 (1H, Py-H_p), 15.4 (2H, Py-H_m), 13.5 (4H, Ar-H_m), 3.6 (2H, Ar-H_p), 1.4 (12H, Ar-*Me*), −6.8 (2H, N=C-*H*). FAB mass spectrum, *m*/*z* 467 [M^+], 432 [M^+-Cl]. Anal. ($C_{23}H_{23}N_3FeCl_2$) calcd: C, 59.00; H, 4.95; N, 8.97. Found: C, 58.65; H, 5.16; N, 8.68. μ_{eff} (Evans Balance): 5.26 BM.

5.3.11. Preparation of (2,6-Diformylpyridinebis(2,6-diethylanil))$FeCl_2$ (19). The procedure as above in (5.3.9) using **7** and $FeCl_2$ gave **19** as a green powder in 76% yield. ^{1}H NMR (CD_2Cl_2, broad singlets are observed in each case): δ 63.2 (2H, Py-H_m), 15.4 (1H, Py-H_p), 14.2 (4H, Ar-H_m), 9.6 (8H, CH_2CH_3), 1.5 (2H, Ar-H_p), −1.0 (12H, CH_2CH_3), −6.0 (2H, N=C-*H*). FAB mass spectrum, *m*/*z* 523 [M^+], 488 [M^+-Cl], 398 [M^+-$FeCl_2$]. Anal. ($C_{27}H_{31}N_3FeCl_2$) calcd: C, 61.85; H, 5.96; N, 8.01. Found: C, 61.97; H, 6.13; N, 7.91. μ_{eff} (Evans Balance): 5.36 BM.

5.3.12. Preparation of (2,6-Diformylpyridinebis(2,4,6-trimethylanil))$FeCl_2$ (20). The procedure as above in (5.3.9) using **8** and $FeCl_2$ gave **20** as a green powder in 76% yield. ^{1}H NMR (CD_2Cl_2, broad singlets are observed in each case): δ 66.8 (1H, Py-H_p), 17.5 (4H, Ar-H_m), 15.0 (2H, Py-H_m), 13.5 (6H, Ar-Me_p), 1.4 (12H, Ar-Me_o), 0.1 (2H, N=C-*H*). FAB mass spectrum, *m*/*z* 496 [M^+], 460 [M^+-Cl], 425 [M^+-2Cl], 370 [M^+-$FeCl_2$]. Anal. ($C_{25}H_{27}N_3FeCl_2 \cdot 0.5H_2O$) calcd: C, 59.43; H, 5.59; N, 8.32. Found: C, 59.12; H, 5.45; N, 8.13. μ_{eff} (Evans Balance): 5.29 BM.

5.3.13. Preparation of (2,6-Diformylpyridinebis(2,4,6-trimethylanil))$CoCl_2$ (21). The procedure as above in (5.3.9) using **8** (0.426 g, 1.15 mmol) and $CoCl_2$ (0.15 g, 1.15 mmol) gave **21** as a golden powder in 65% (0.354 g) yield. ^{1}H NMR (CD_2Cl_2, broad singlets are observed in each case): δ 88.0 (2H, Py-H_m), 14.3 (1H, Py-H_p), 7.3 (6H, p−CH_3), 0.1 (2H, N=C-*H*), −2.2 (4H, Ar-H_m), −19.6 (12H, Ar-Me_o). FAB mass spectrum, *m*/*z* 500 [M^+], 464 [M^+-Cl], 429 [M^+-2Cl], 370 [M^+-$CoCl_2$]. Anal. ($C_{25}H_{27}N_3CoCl_2 \cdot 0.5H_2O$) calcd: C, 59.07; H, 5.55; N, 8.27. Found: C, 59.25; H, 5.40; N, 8.28. μ_{eff} (Evans Balance): 4.66 BM.

5.4. Complexation with $FeCl_3$. Preparation of (2,6-Diformylpyridinebis(2,4,6-trimethylanil))$FeCl_3$ (22). To a solution of $FeCl_3$ (0.100 g, 0.615 mmol) in MeCN (50 mL) was added **8** (0.227 g, 0.615 mmol). After the solution is stirred at room temperature overnight, a precipitate is formed. Filtration and washing with diethyl ether (3 × 30 mL) gives **22** as red solid in 61% yield (0.201 g). FAB mass spectrum, *m*/*z* 532 [M^+], 497 [M^+-Cl], 461 [M^+-2Cl]. Anal. ($C_{25}H_{27}N_3FeCl_3$) calcd: C, 56.44; H, 5.08; N, 7.90. Found: C, 56.08; H, 4.96; N, 7.61.

5.5. Analysis of Decomposition Products from 9 with MAO 5.5.1. With 100 Equivalents of MAO. To a solution of **9** (0.015 g, 0.025 mmol) in toluene (30 mL) was added MAO (100 equiv, 1.43 mL, 2.5 mmol). The orange solution was maintained stirring at 50 °C for 1 h. The solution was cooled to 0 °C, and methanol was added followed by dilute HCl (10%). The organic layer was separated, dried over $MgSO_4$, and dried in vacuo. ^{1}H NMR in $CDCl_3$ indicated the presence of free 2,6-diacetylpyridinebis(2,6-diisopropylanil) **1** as the only ligand component.

5.5.2. With 1000 Equivalents of MAO. Using the procedure above in (a) but introducing 1000 equiv of MAO (14.3 mL, 25 mmol) yielded ^{1}H NMR consistent with **1** as the only ligand component after workup.

5.5.3. Ten Minute Polymerization with 100 Equivalents of MAO. To a solution of **9** (0.015 g, 0.025 mmol) in toluene (30 mL) was added MAO (100 equiv, 1.43 mL, 2.5 mmol). The orange solution was stirred for 5 min at room temperature and ethylene introduced (1 bar). After 10 min at room temperature, the polymerization was terminated by the addition of methanol and dilute HCl (10%) at 0 °C. The solid polethylene was filtered, the organic layer was separated from the filtrate and dried over $MgSO_4$, and the solvent was stripped off. ^{1}H NMR in $CDCl_3$ indicated only the presence of free **1** as the only ligand component.

5.6. General Polymerization Procedures. 5.6.1. High-Pressure Tests. A 1 L stainless steel reactor was baked out under a nitrogen flow for at least 1 h at >85 °C and subsequently cooled to the temperature of polymerization. Isobutane (0.5 L) and trialkylaluminum (triisobutylaluminum or trimethylaluminum) were introduced into the reactor and stirred at reaction temperature for at least 1 h. Ethylene was introduced into the reactor by back pressure of nitrogen. The catalyst solution in toluene was then injected under nitrogen. The reactor

pressure was maintained constant throughout the polymerization run by computer-controlled addition of ethylene. The polymerization time was between 12 and 60 min. Runs were terminated by venting off volatiles, and the reactor contents were isolated, washed with aqueous HCl and methanol, and dried in a vacuum oven at 50 °C.

5.6.2. Schlenk-Line 1 Bar Ethylene Tests. The precatalyst was dissolved in toluene (40 mL) and MAO (10 wt % in toluene) added to produce an orange solution. The Schlenk tube was placed in a water bath and purged with ethylene, and the contents were magnetically stirred and maintained under ethylene (1 bar) for the duration of the polymerization. The polymerization was terminated by the addition of aqueous hydrogen chloride. The solid PE was recovered by filtration, washed with methanol (50 mL), and dried (vacuum oven at 50 °C).

5.7. Determination of Vinyl Content by IR Spectroscopy. Vinyl contents of polymers obtained by polymerization of ethylene using complexes **9**, **15**, **16**, and **17** are listed in Table 2.

For each sample, the PE powder (∼20 mg) was pressed to give a thin film (thickness ∼100 μm) suitable for IR examination. The vinyl content was calculated from the intensity of the peak at 910 cm^{-1}, taking as background the average of the absorbance on either side of the peak. The extinction coefficient used for this peak was 120.[29]

5.8. X-ray Crystal Structure Determinations of 9, 11, 12, and 14. Table 7 provides a summary of the crystal data and data collection and refinement parameters for compounds **9**, **11**, **12**, and **14**. The structures were solved by direct methods, and the non-hydrogen atoms were refined anisotropically by full matrix least-squares based on F^2. The C−H hydrogen atoms of the methyl groups bound to *sp* or sp^2 centers were located from ΔF maps, idealized, assigned isotropic thermal parameters, $U(H) = 1.5U_{eq}(C)$, and allowed to ride on their parent atoms. The remaining C−H hydrogen atoms were placed in calculated positions, assigned isotropic thermal parameters, $U(H) = 1.2U_{eq}(C)$ [$U(H) = 1.5U_{eq}$(C-Me)], and allowed to ride on their parent atoms. The O−H hydrogen atoms in **9** and **14** could not be located. Computations were carried out using the SHELXTL PC program system.[67]

The crystallographic data (excluding structure factors) for the structures reported in Table 7 have been deposited with the Cambridge Crystallographic Data Center as supplementary publication number CCDC 134109-134112. Copies of the data can be obtained free of charge on application to The Director, CCDC, 12 Union Road, Cambridge, CB12 1EZ, UK (Fax, Int. code +(1223)336−033; e-mail, teched@chemcrys.cam.ac.uk).

Acknowledgment. BP Amoco Chemicals Ltd. is thanked for financial support. Drs. J. Boyle and G. Audley are thanked for NMR, IR, and GPC measurements, and Professor D. M. L. Goodgame is thanked for his helpful discussions.

JA990449W

(67) SHELXTL PC version 5.03, Siemens Analytical X-ray Instruments, Inc., Madison, WI: 1984.